

Emergent Workload Inequality in Collective Excavation

Laura K. Treers¹, Aradhya Rajanala², Nathan Nguyen³, Naomi Wagner⁴, Michael A. D. Goodisman⁵, Daniel. I. Goldman²

Abstract

Collectives of entities, including groups of living systems and artificial swarms, self-organize to achieve common goals. Collective systems frequently employ a division of labor, wherein individuals take on different tasks or perform different amounts of work. However, the rules and mechanisms used by collectives to divide labor remain poorly understood. In this study, we investigate the methods used by biological collectives to complete tasks using experimental and theoretical approaches. We use social insects, which form remarkably integrated societies, as model systems to study division of labor. We specifically explore how workload inequality might arise by studying digging behavior in *Solenopsis invicta* fire ants. We introduce an experimental technique for estimating each ant’s workload by tracking individual grain depositions during digging behavior. These experimental results suggest that workload distribution becomes more unequal for increasing group size. We then implement an agent-based cellular automata model which predicts experimental trends, and suggests that local decisions driven by crowding emergently account for the scaling of workload inequality. Finally, we examine experimental workload results and show that the number of “active” digging ants roughly scales with the square root of the total group size. This finding parallels scaling laws from other domains of social and natural science, such as Price’s law, which suggest that a core group of individuals perform the majority of work. We introduce a simplified rate equation model which recovers the square root scaling via a quadratic failure rate. Together, these results provide a mechanistic explanation for the emergent workload scaling patterns in collectives.

I. INTRODUCTION

In biological and robotic collective systems, many individuals work together to achieve complex tasks. Individuals in some biological collectives operate in a decentralized capacity, using local information to inform decision making. Nevertheless, simple rules followed by many individuals often lead to complex, effective group behaviors; for example, flocks of birds [1] and schools of fish [2] coordinate their movements to conserve energy, evade predation, and share information [3]. These collective systems often operate under the presence of constraints: such constraints include space restrictions, in the case

¹ Dept. of Mechanical Engineering, University of Vermont ² School of Physics, Georgia Institute of Technology ³ School of Physics, California Institute of Technology ⁴ Department of Physics, Oglethorpe University ⁵ School of Biological Sciences, Georgia Institute of Technology

of collective construction [4], or limited resources, in the case of group foraging [5]. Throughout evolutionary history, biological systems have evolved strategies for maintaining effective collective behaviors despite the presence of these constraints.

One general principle employed by collective systems operating under constraints is division of labor [6]–[8]. Such specialization occurs when different individuals within a society have distinct roles or take on different amounts of work. Division of labor has been shown to be an important factor in the success of many social species in biology [9], [10]. Moreover, variation in individual contributions in work effort could arise through a variety of factors across collective systems [11]–[14]. However, the mechanisms leading to variation in individual behavior and division of labor among individuals remain poorly understood [15].

One of the most successful classes of collective systems is social insects, which include ants, termites, some bees, wasps, thrips, beetles, and aphids. In social insect colonies, individuals coordinate activities and behave as a single ‘superorganism’ [16]–[18]. These social insects represent only two percent of insect taxa but account for more than half of total insect biomass [19], [20]. One of the main reasons social species are so successful is the high level of division of labor within colonies [10], [21], [22]. One family of social insects, Formicidae, or ants, represent one of many independent examples of the evolution of sociality in insects. Similar to many other social insects, ants live in large colonies and must coordinate to achieve various tasks necessary for survival, such as nest construction.

Nests are fundamentally important to the success of ant species, and the behaviors leading to the successful construction of these nests are remarkable [23]–[31]: thousands of low-level individual interactions result in functional, space filling structures [5], [23], [26], [32]–[36]. One ant species known for complex nest construction is *Solenopsis invicta* (hereafter the ‘fire ant’) [37]. Fire ants are master builders, successfully excavating various soils found around the world [38]–[42]. Fire ants build nests comprised of a network of subsurface branching tunnels (Figure 1A).

Nest construction necessitates division of labor: individuals must coordinate activities to successfully manipulate and shape the environment [9], [43]–[45]. Prior studies have shown that individual contributions to the single task of nest excavation are highly unequal, both in laboratory and in field studies [12]. In fact, a large percentage of a colony of workers at any given time is completely inactive [21], [46]. In fire ant excavation, 30% of workers complete approximately 70% of the total work [4]. Recent studies have shown that this behavior is adaptive: using both cellular automata as well as robophysical models, Aguilar et al. showed that fire ants’ unequal workload distribution optimized traffic flow, reducing jams and increasing excavation speed [4]. Other studies have demonstrated that the presence of these inactive workers may also increase the long-term persistence of the colony [47].

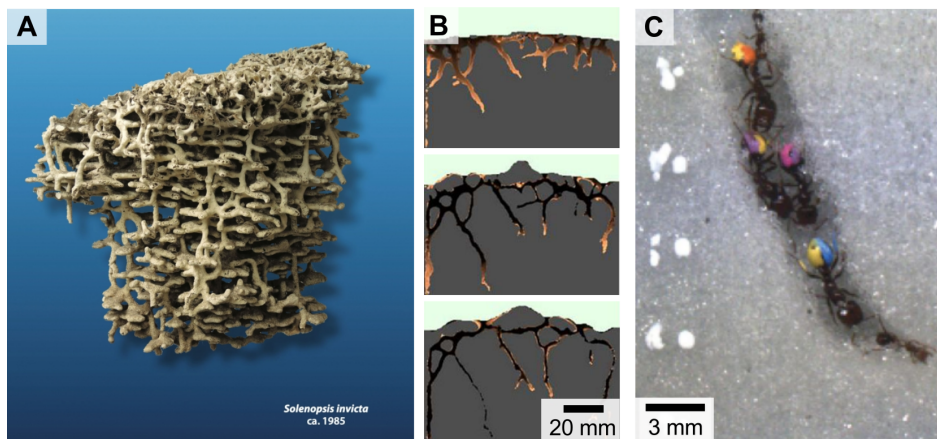


Fig. 1: **Image of fire ant nest construction.** (A) Cast of a fire ant (*Solenopsis invicta*) nest, created by Walter Tschinkel. The nest is approximately 40 cm in diameter, and consists of a complex array of narrow, branching tunnels. Adapted from [53]. (B) Tunnel excavation in a 2D “ant farm” experiment, over 9 hours, adapted from [54]. Each image represents a 3 hour slice of ant activity. Tunnel color represents first-exploration time, ranging from darkest for earliest and brightest for latest activity within the time slice. (C) A group of fire ants excavates grains at the end of a narrow tunnel. Adapted from [4].

How global workload inequality emerges from local interactions is not well understood. The origins of this workload inequality might be explained via two disparate hypotheses: 1. Certain characteristics of ants makes some intrinsically less likely to contribute such that they “specialize” in inactivity [46] (for example, they are immature workers [48]) or 2. Workers are not intrinsically different; rather, other factors, such as environmental conditions, create a self-regulating phenomenon in which some ants choose to remain inactive. Several studies have investigated these hypotheses via mathematical models [49]–[52]. Many of these studies have remained in simulated environments, and have focused on colony-level behavioral trends. However, recent results suggest that individual interactions in crowded environments affect resultant traffic flow [4].

Thus, we hypothesize that the mechanisms underlying workload inequality might be driven by local interactions in the tight tunnels in which the ants operate (Figure 1B-C). These tunnels are consistently narrow (approximately 2 ant body widths wide) across a range of substrates [40]. Further, we hypothesize that by studying behavior of smaller ($10^1 - 10^2$) groups of individuals in the crowded environment of early nest construction, we can probe the pressures that lead to inactivity in these smaller groups, and thus result in widespread workload inequality in the larger collective. A systematic way to understand the role of crowding and confinement in workload inequality is to vary the group size in a fixed experimental area [55]. In this study, we experimentally vary group size to determine how crowding affects workload distribution. We show that inactivity scales sublinearly with group size; in particular, we show that the

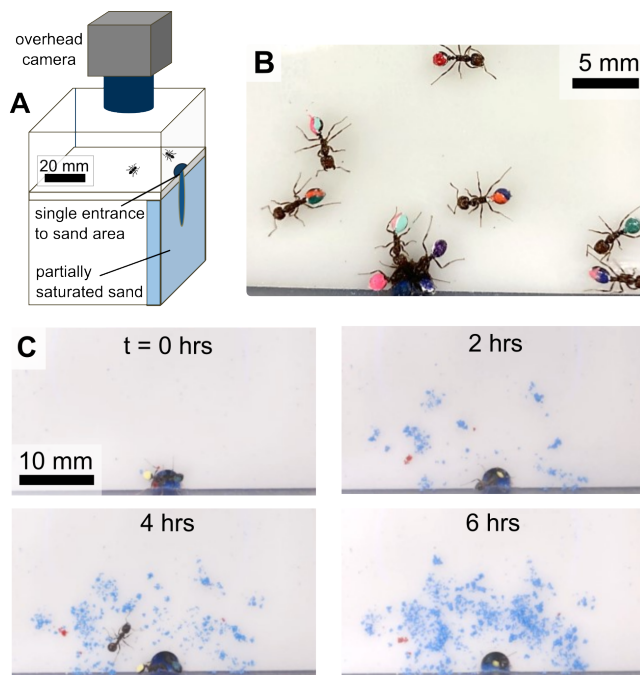


Fig. 2: **Painting ants enables individual ant tracking.** (A) Diagram of camera and container used to record simultaneous experimental trials. (B) Painted and color-coded ants used in trials with more than 10 individuals. (C) Camera view of trial at 4 different points in time over 6 hours.

number of active ants in a given group scales as the square root of the total group size. Using both our experimental and cellular automata simulation methods, we argue that self-regulation of activity may be modulated by encounter rate or relative density of individuals in a tunnel. Through a mechanistic model, we then show how this square root scaling might emerge in constrained collective systems.

II. RESULTS

A. Experimental Setup

Several *Solenopsis invicta* fire ant colonies were collected from locations in the metro Atlanta, GA area. The colonies were maintained in a climate controlled room on the Georgia Tech campus. Colonies were fed a protein-carbohydrate mixture 2x weekly and supplied a constant water source via cotton-covered tubes. To study digging behavior, plastic containers ($\approx 65 \times 65$ mm), shown in Figure 2A, were prepared such that a small region of width ≈ 2 mm along one edge was filled with partially saturated colored sand (saturated 20% by mass, grain size distribution 75 - 400 μm). A 4 mm diameter hole on the side of a plastic covering enabled ants to enter the sand, but restricted entrance and exiting of this region to a single location. Doing so enabled monitoring when each ant entered and exited the artificial “nest” region (and thus served as a proxy for each ant’s activity).

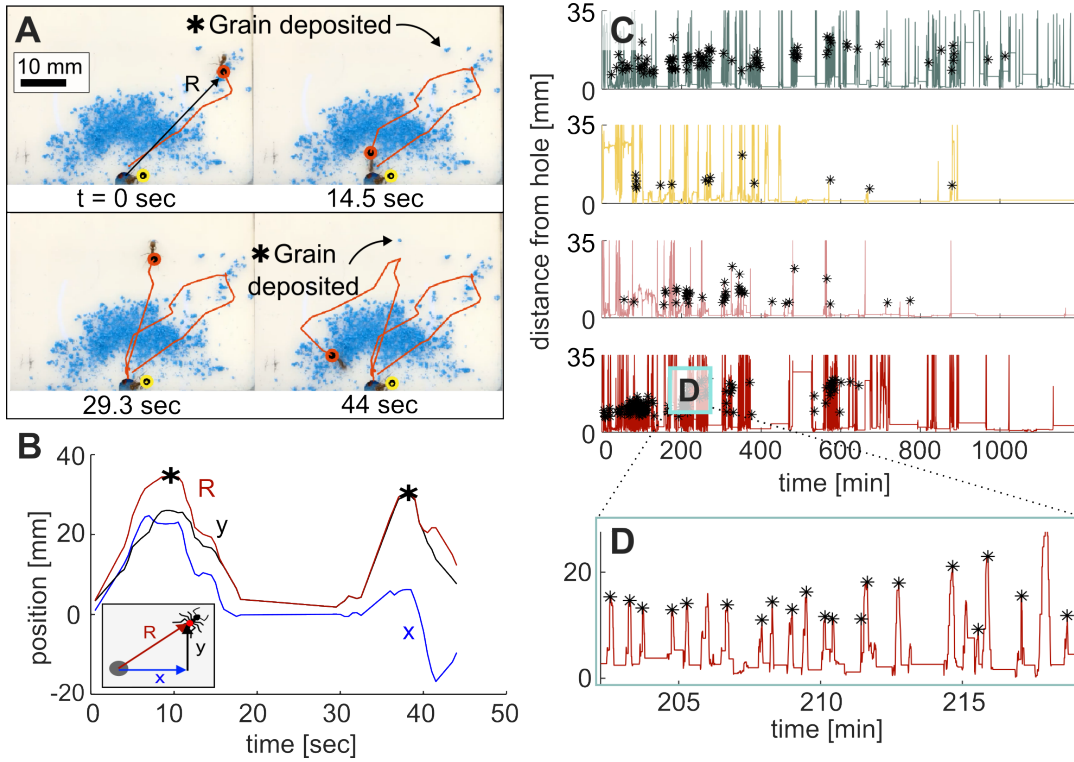


Fig. 3: **Automated high throughput ant tracking method for estimation of grain deposition events.** (A) Lines representing tracked path of a single (red) ant across 44 seconds. (B) The corresponding horizontal position (x), vertical position (y) and distance from the tunnel entrance over time for the same ant. Asterisks indicate the local maxima in radial distance, which the tracking algorithm denotes as grain depositions. (C) Ant positions, as represented by distance from tunnel opening, over time for the 4 ants in a single trial. (D) A representation of the position data in (C), for a single ant across ≈ 15 mins. Black asterisks represent points automatically identified as a grain deposition based on the thresholding process described in Section II-A.1

Each day, workers were randomly selected from a single colony and their gasters were painted with color codes for purposes of video identification (Figure 2B). New containers were prepared daily, and in each container, we placed 2, 3, 4, 6, 10, 15, 20, or 25 ants. Each trial was started between 4 PM and 6 PM daily, and the containers were randomized such that the same number of ants were not always placed into the same container each day. An array of cameras (Logitech C920) were set up to record overhead videos of each trial for 20 hours. Sample overhead images of pellet depositions over six hours are shown in Figure 2C. Ants were not returned to the colony after each trial.

1) *Video analysis techniques:* Custom MATLAB scripts were designed to analyze the videos resulting from each trial. For trials with 10 or fewer ants, individual ant locations were tracked via an algorithm which performed color thresholding to identify gaster paint on each ant. Further detail on the identification of ant locations from video data is included in Materials & Methods. A secondary custom MATLAB script converted individual ant positions to radial distances from the tunnel entrance, shown

in Figure 3A-B. An increase and subsequent decrease in radial distance was presumed to represent an ant leaving the tunnel, depositing a grain, and subsequently returning to the tunnel. The script selected these events by identifying local maxima in radial distance data. From visual observation, we identified a minimum distance from the hole which represented a viable “trip” from the tunnel with a grain (≈ 6 mm), as well as a maximum distance, above which the ant most often exited the camera view and did not return to the tunnel entrance (≈ 28 mm). Based on visual observation, we also set a maximum time frame for an exit, grain deposition, and return to the tunnel as 12 seconds. Local maxima which met all of the distance and time criteria described above were counted as grains deposited by that ant. Using this technique, the script tracked each ant’s contributions to tunnel construction via the number of grains it deposited over the course of the trial, shown in Figure 3C-D. This automated technique was used for ant group sizes of 10 or fewer; for the trials with 15 or more ants, this custom technique was insufficient for tracking multi-color coded individuals, and thus activity during the first 8 hours of these trials was tracked manually.

B. Experimental Results

Using the aforementioned video analysis strategy, we denoted the time and location of each ant’s grain deposition events over the course of each trial. A sample trial for 4 ants is shown in Figure 4. The number of deposited pellets increased sharply during the first ≈ 5 hours for each ant. The rates of

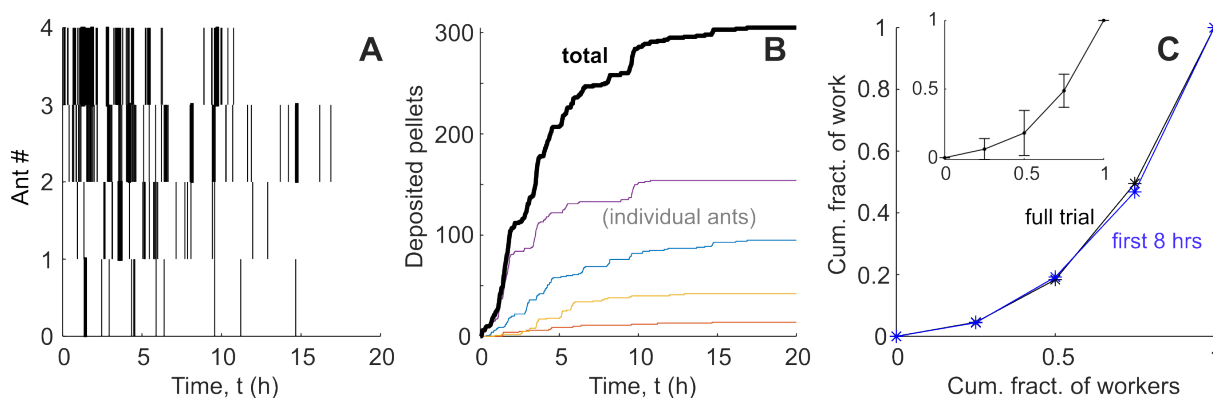


Fig. 4: **Workload inequality is revealed via Lorenz curve analysis of deposition events.** (A) Plots of ant activity over the trial duration where a black dash indicates a grain transported at that time instance. Each row corresponds to a different ant, with the top row corresponding to the most active ant. Ants are ordered by total activity over 20 hours. (B) Number of deposited pellets, as estimated by the tracking algorithm, for each ant across 20 hours. Colored lines represent individual ant contributions, while the black curve represents the total pellets deposited. (C) Lorenz curves, representing cumulative fraction of grains moved, relative to cumulative fraction of workers involved, for the first 8 hours (blue) and full 20 hour trial (black) for these 4 ants. Inset shows mean Lorenz curve over all 4 trials, with error bars representing standard deviation.

deposition (and thus, tunnel excavation) decreased drastically afterwards and settled to a slower long timescale behavior. This mirrors results found by Avinery et al. [54] for tunnel growth trends in larger (40 - 70) groups of ants. Similarly, Figure 4A shows the relative level of activity across the trial – black bars represent active time periods in which grains are transported. The activity started high for multiple ants and decreased over time. This trend is also reflected in the cumulative number of deposited pellets over time (Figure 4B).

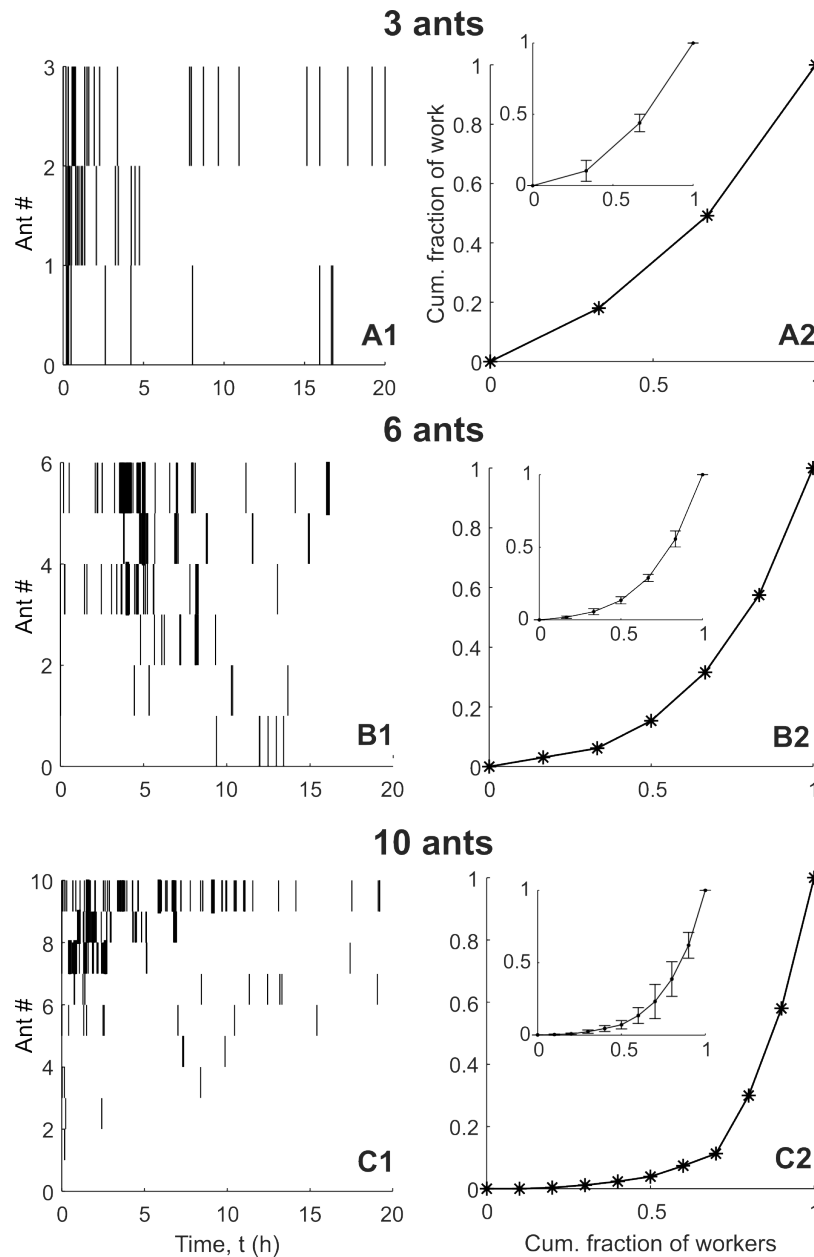


Fig. 5: **Increasing group size leads to greater workload inequality.** (A1) Individual ant activity, as indicated by black dashes, sorted from highest to lowest total activity. (A2) Lorenz curves for the corresponding trial for 3 ants. Insets show mean Lorenz curves over 4 trials (error bars represent standard deviation). Representative trials are also shown for 6 (B1-2) and 10 (C1-2) ants.

We then investigated how participation, and thus workload, trends evolved throughout these trials. The cumulative fraction of work (approximated by the pellets deposited) completed by a cumulative fraction of ants is shown in Figure 4C. This relationship, also known as a Lorenz curve [4], represents the level of “unequalness” in workload for this particular trial. Perfectly equal workload distribution, or a line of equality, would be represented by a straight line connecting (0,0) to (1,1). Using the experimental Lorenz curves, we calculate the Gini coefficient, or G , defined as the ratio of the area between the Lorenz curve and the line of equality to the area under the line of equality. The Gini coefficient represents the deviation of the workload from perfectly equal ($G = 0$, all ants work equally) to completely unequal ($G = 1$, a single ant performs all work). Figure 4C demonstrates that unequal workload distributions are preserved throughout the entire trial.

We then compare trends in workload distribution across varying group size. As shown by three representative trials in Figure 5, as the group size increases, the workload distribution becomes increasingly unequal. For the smaller group sizes tested, nearly all ants participated to some degree (Figure 5A2). However, for larger group sizes, we observe an increasing fraction of ants which perform little to no excavation, and instead a core group of ants perform all digging (Figure 5C2). We then compare trends over all group sizes; the resultant Gini coefficients for the first 8 hours of all trials are represented in Figure 6. We observe a sublinear, monotonically increasing trend in Gini coefficient with increasing group size. If extrapolated, this trend predicts the Gini coefficient range for 30 ants which was predicted by Aguilar et al. ($G = 0.81 \pm 0.15 - 0.83 \pm 0.16$) [4].¹

This trend supports initial observations that large groups not only share work highly unequally (as observed in prior literature), but that this workload inequality increases the larger the group becomes. To better understand the mechanisms underlying this observation, we implement an agent-based model which captures the role of individual ant decision making in a simplified tunnel environment.

¹Aguilar et al. used only the ants which appeared in the camera frame at the end of the tunnel to calculate Gini coefficient; thus, their estimates do not take into consideration the inactive workers in the group, while our estimates consider all workers. They report that a fraction of the 30 ants (between 0.22 ± 0.1 and 0.31 ± 0.13) never visited the tunnel face in their experiments, and report a Gini coefficient $G = 0.75 \pm 0.1$. In our formulation, this corresponds to an effective Gini coefficient range of $G = 0.81 \pm 0.15 - 0.83 \pm 0.16$.

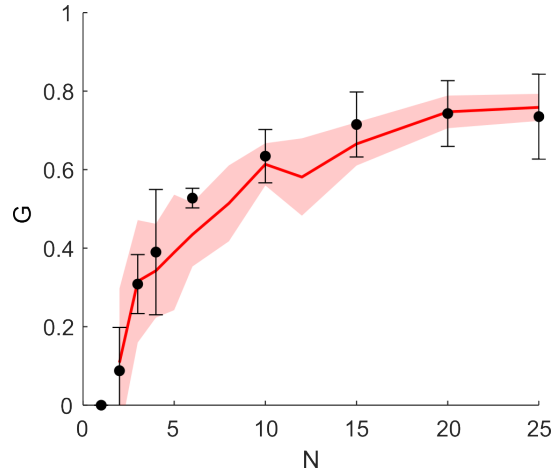


Fig. 6: **Gini coefficient scales sublinearly with group size.** Black dots represent experimental Gini coefficients, G , as a function of group size, N , derived from Lorenz curves in Figure 5. Error bars represent standard deviations over 4 experimental trials (<10 ants) or 3 experimental trials (≥ 10 ants). Red curve represents mean Gini coefficients resulting from the CA simulation in Section II-C, for a single choice of parameters ($R = 0.1$, $\tau_0 = 10$, $C_0 = 1$, $\tau_s = 2$). The shaded region represents standard deviation over 10 simulation trials performed at each group size.

C. Cellular Automata Simulation

1) *CA Model Formulation:* To better understand the role of environmental factors in regulating behavior, we build a cellular automata (CA) simulation [4], [54]. In this simulation structure, each “cell” can be occupied by one of three states: unexcavated substrate in the tunnel, empty (excavated) space in the tunnel, or an ant. The model ants in the simulation move through a series of states, as regulated by various factors, shown in Figure 7. Starting with the ants “outside” of the tunnel region, each ant has a probability P of entering the tunnel. Once inside the tunnel, the ants move forward one cell each timestep and have a fixed probability, 0.52, of also moving laterally, as observed experimentally in prior work [4]. If at any point, an ant cannot locomote forward, it either remains in place until space is made, or reverses with probability 0.34 [4]. If the ant reaches the end of the tunnel, it removes a pellet, then exits the tunnel and deposits the pellet. The time required to excavate a pellet, the number of pellets required to remove a CA cell, and the time required to deposit a pellet are all constants which were derived from experimental observation in prior work [4], [39], [54]. After an ant deposits a pellet, the cycle repeats again and the ant has probability P of re-entering the tunnel. Further CA implementation details, including all constants, are described in the Materials & Methods.

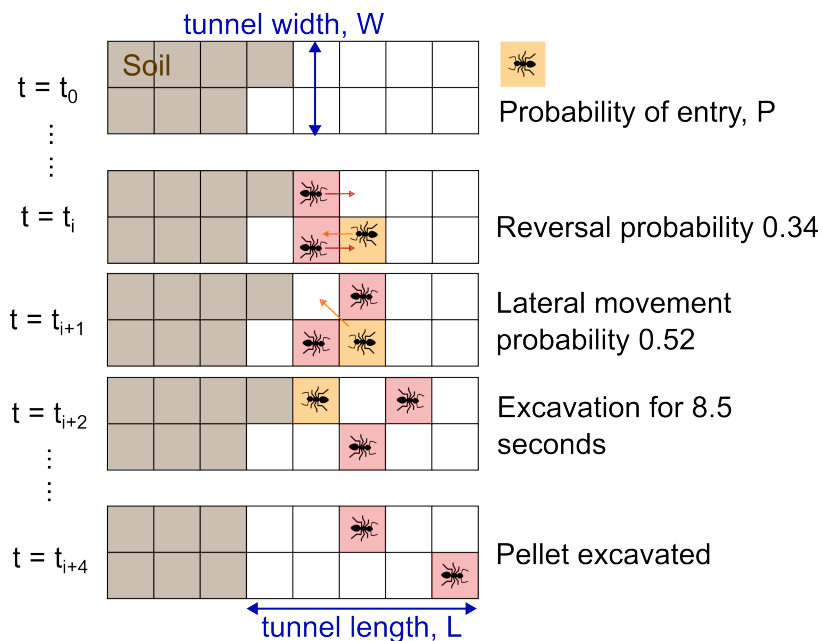


Fig. 7: **Cellular automata simulation layout and algorithm.** Depiction of steps in the excavation of a pellet in the CA simulation, beginning with an ant entering the tunnel with probability P , and ending with a pellet excavated and removed from the tunnel. Brown cells represent unexcavated soil in the tunnel, white cells represent already excavated tunnel, orange cells represent ants moving toward the end of the tunnel (left), and red cells represent ants moving towards the tunnel entrance (right).

Prior work revealed that during early nest excavation, an ant’s probability of entering the tunnel may be modeled by a self-limiting process, which can be effectively described by a “work-rest imbalance.” In other words, this imbalance, t_{imb} , characterizes how far an ant has deviated from its preferred ratio of work to rest. As described in prior work [54], an ant’s work-rest imbalance can be defined as $t_{imb} = t_{work} - Rt_{rest}$, where t_{work} and t_{rest} represent the amount of time an ant has spent working and resting, respectively. R represents an individual’s intrinsic preferred work-rest ratio. Furthermore, this work-rest imbalance can be used to infer an ant’s probability of entering the tunnel and engaging in nest construction. In line with prior work, we use this imbalance to define a probability of entry, P_0 , which scales with the work-rest imbalance as $P_0 = e^{-t_{imb}/\tau_0}$, where τ_0 a timescale for the tolerance of a work-to-rest imbalance [54]. According to these definitions, if an ant has rested more than its intrinsic ratio would dictate, it will tend to enter and engage, and in contrast, working more than usual will be more likely to result in resting behavior.

However, this definition for probability of participation only takes into account an ant’s intrinsic willingness to work, R , and is not inherently regulated by other potential external factors, such as crowding and confinement. When implementing only P_0 as the probability of entry, assuming all ants have equal R , net participation over long timescales is nearly equivalent across individuals, which is not

representative of experimental results. Instead, we incorporate the role of local crowding information, such as the encounter rate, into individual ants' decision making [54], [56]. We introduce a term which scales the entry probability by the local success rate of movement in the tunnel. Thus, the probability of entering the tunnel and engaging in nest construction, P , can be defined as $P = e^{-1/(lC_0)}P_0$ where C_0 is a crowding sensitivity parameter and l is the success rate of moving forward in the tunnel. This success rate is calculated as an exponential moving average with memory τ_s timesteps. Thus, if an individual ant is entirely unsuccessful at moving forward in the tunnel within τ_s timesteps, its probability of entry will be zero and it will stop trying to enter the tunnel. In contrast, an ant in an uncrowded environment will be largely unaffected by this additional parameter (its entry probability would be universally scaled by e^{-1/C_0}).

2) *CA Simulation Results:* As shown in Figure 8, for one choice of parameters ($R = 0.1$, $\tau_0 = 10$, $C_0 = 1$, $\tau_s = 2$), this CA simulation captures overall trends in excavation performance. We observe that in simulation, a group of 3 ants will share workload nearly equally, but in a group of 6 or 10 ants, the work is done by a subset of active workers, and the size of this group does not scale linearly with the total group size. Thus, this simulation effectively demonstrates that the portion of inactive ants will increase with group size. As shown in Figure 6, for the same choice of parameters, this CA structure is able to capture the experimental relationship between group size, N , and workload distribution. However, the variability in simulated Gini coefficient decreases with increasing group size, which is not reflected in the experimental data.

Overall, the simulated ant activity is less stochastic than that observed in experiments: in the simulation, ants which are active tend to excavate throughout the entire trial, and those which stop excavating tend to have little no activity for long durations. This tendency results in Lorenz curves for the simulation which are largely comprised of straight line segments (Figure 8) – there is a long flat “tail” comprised of inactive or nearly inactive ants, and a diagonal straight line segment which represents the active ants, which often perform similar levels of work. This tendency to continuously engage or disengage from excavation is likely a byproduct of the short “memory” of ants in simulation, dictated by the memory timescale $\tau_s = 2$. In other words, a short memory means that ants are quick to decide whether or not to engage in digging based on local crowding conditions, and these decisions persist throughout the trial.

3) *CA Parameter Sensitivity:* We next seek to understand how sensitive the simulation results are to changes in individual parameters, and thus probe the role of individual mechanisms in emergent collective behavior. We run a set of simulations in which we systematically sweep over each simulation parameter individually, and otherwise use a set of default parameters ($R = 0.1$, $\tau_0 = 10$, $C_0 = 1$, $\tau_s = 2$). The results of this parametric sweep are shown in Figure 9. We observe that the Gini coefficient

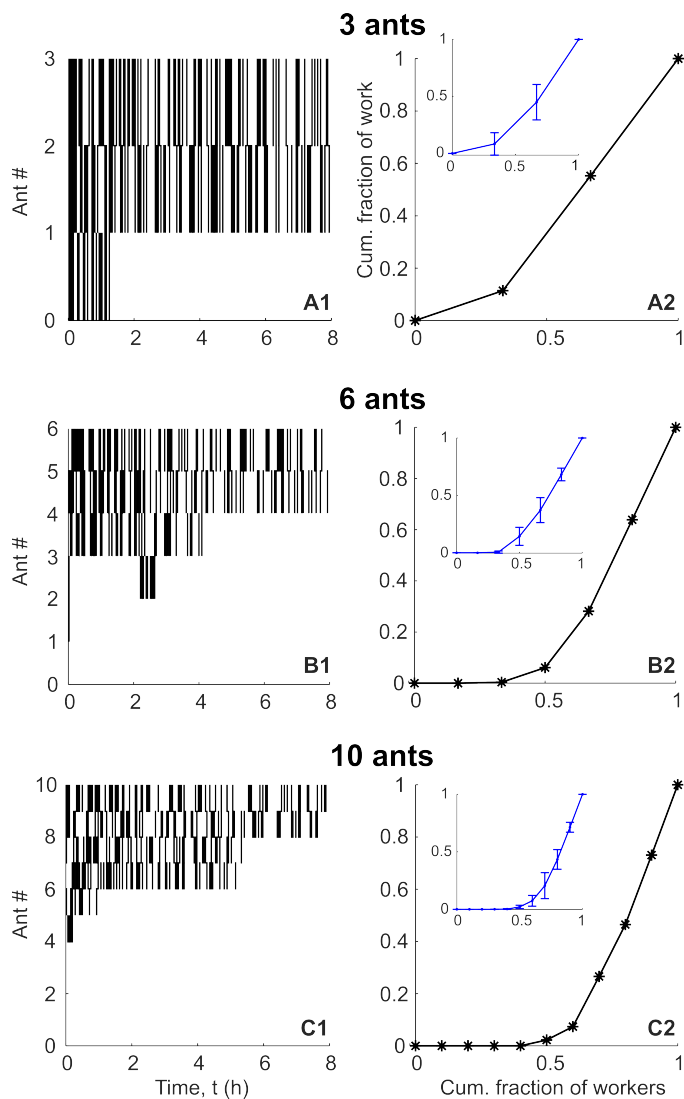


Fig. 8: **CA Simulation captures correlation between group size and workload inequality.** (A1) Individual ant activity in the CA simulation, as indicated by black dashes, sorted from highest to lowest total activity. (A2) Lorenz curves for the corresponding simulation trial, for 3 ants. Insets represent mean Lorenz curves over 10 simulation runs for one set of simulation parameters ($R = 0.1$, $\tau_0 = 10$, $C_0 = 1$, $\tau_s = 2$). Representative trials and mean Lorenz curves are also shown for 6 (B1-2) and 10 (C1-2) ants.

trends are largely insensitive to the crowding sensitivity parameter C_0 , as well as the timescale for the tolerance of a work-rest imbalance, τ_0 . The simulation results for sweeps over these two parameters are contained in the Supplemental Information. However, we do observe a dependence of Gini coefficient on memory parameter τ_s , as well as the intrinsic work-rest ratio, R . We observe that in order to effectively reproduce experimental trends in Gini coefficient, a short timescale ($\tau_s = 2$) is necessary, corresponding to a memory of approximately 7.4 seconds based on the simulation timestep used in this work (Figure 9A). We hypothesize that in order to maintain an appropriate rate of crowding-induced deactivation, the

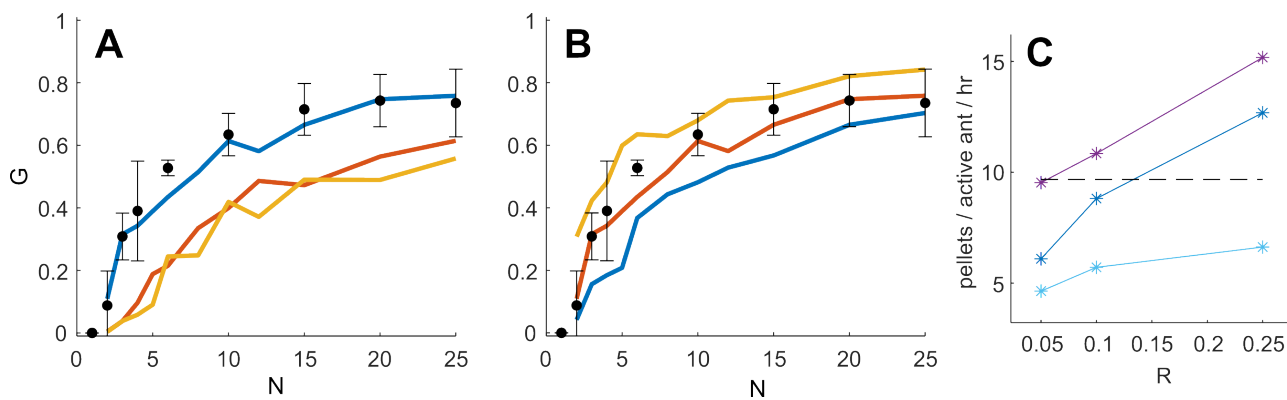


Fig. 9: **Effect of simulation parameters on workload distribution and excavation rates.** (A) The effect of memory parameter τ_s on resulting mean Gini coefficient, across all group sizes, N , in simulation (colored lines). Blue, red, and yellow curves represent $\tau_s = 2, 5, 10$, respectively. Experimental measurements are shown with black dots and error bars. (B) The effect of intrinsic work-rest ratio, R , on mean Gini coefficient trends. Blue, red, and yellow curves represent $R = 0.05, 0.1, 0.25$, respectively. (C) The effect of simulation parameters on excavation rates (colored lines) vs. mean experimental excavation rate (dashed black line). From bottom to top, colored curves represent τ_0 & $C_0 = 1, 10, 100$, respectively.

ants in simulation are effectively “impatient,” persisting only for short periods in crowded conditions before their probability of re-entry diminishes. We also observe that for higher intrinsic motivation, R , we observe increasingly unequal workload distribution (Figure 9B). We hypothesize that if ants have a higher baseline likelihood of entering the tunnel (higher R), the tunnel will become more crowded, leading to increased levels of crowding-induced “deactivation.” In contrast, if ants have a low baseline motivation, there will be less ants entering the tunnel and less crowding. As a result, more ants are able to participate in excavation throughout the trial without persistent roadblocks.

We also investigate how the parameters introduced in this simulation affect excavation rates. Prior work has shown that total excavated tunnel area (and by association, the number of excavated pellets) scales linearly with the total number of active ants [39]. Thus, we compute the total number of active ants in each hour of the simulation for each combination of parameters. We then compare the mean number of active ants to the total number of pellets excavated in each trial and fit a linear excavation rate, measured in pellets excavated per ant per hour. Figure 9C shows the excavation rates predicted by the simulation for three combinations of parameters and shows how the ants’ intrinsic motivation, R , is strongly correlated with resulting excavation output. Overall, we observe that for all parameters tested, the simulation excavation rates are within $\pm 50\%$ of experimental values. The role of each individual parameter on excavation rates, as well as details of how excavation rates were approximated, are described further in the Supplemental Information.

D. Theoretical Analysis

Both the experimental and simulation results demonstrate a consistent, sublinear relationship between group size and Gini coefficient. To further understand the origin of this trend, we approximate a relationship between Gini coefficient and net participation in a group. Given prior observation that some subset of ants within a group is active while the rest remain primarily inactive, we choose to create a simplified definition for Gini coefficient. Shown in Figure 10A, we assume that a typical Lorenz curve can be reduced to two straight line segments: one which captures the low activity in the inactive subset of ants, and a second, steeper line segment which captures the majority of work completed by the “active” ants. Thus, we assume that some subset, n , of active ants, completes portion W of the total work done. With this simplification of the Lorenz curve, we can directly relate Gini coefficient (G) to the number of active ants (n) by:

$$G = W - \frac{n}{N} \quad (1)$$

Using this relation, we then convert experimentally derived Gini coefficients to an estimated number of active ants for each group size. We assume that the active ants complete nearly all of the total work ($W = 1$). When comparing the approximated number of active ants, n , to group size, N (Figure 10B), we observe that the number of active ants scales as the square root of the total group size, or that $n \propto \sqrt{N}$.

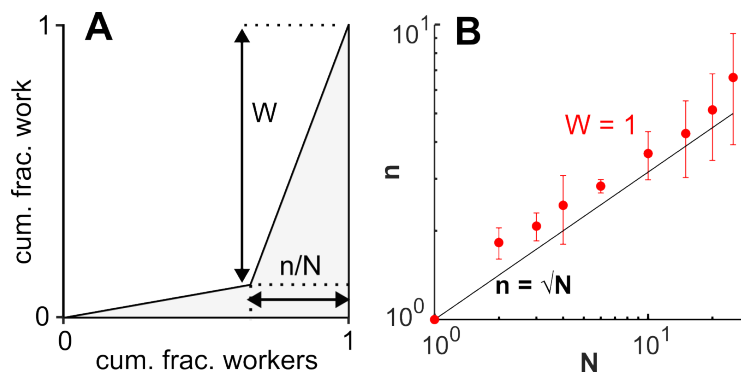


Fig. 10: **Participation trends are captured by a square root scaling relation.** (A) A simplified version of the Lorenz curve in which we assume that a subset of active ants, n , contribute equally to the excavation, performing fraction W of the total work. (B) Using a simplified form for approximating Gini coefficient from the Lorenz curve (shown in A), we estimate the total number of active ants from the measured Gini coefficients, assuming $W = 1$. Red points with error bars represent means and standard deviation over 4 trials (2-6 ants) and over 3 trials (10 - 25 ants). Solid line represents the case where n scales as the square root of N .

1) *Analytical approach to model participation rates:* To identify a physical mechanism and biological motivation for this square root scaling, we develop a simplified model for ant participation in digging

using a rate equation methodology [57]. This model simplifies the cellular automata model by abstracting ant movement within the tunnel as a stochastic process. We introduce a model tunnel environment which, similar to the cellular automata, is 2 cells wide and L cells long. We assume that the number of ants in the tunnel at any given time, n , corresponds to the number of active ants in the collective, and that the tunnel is sparsely filled ($n \ll L$). The total number of ants in the model is N , some of which are within the tunnel (active) and some of which are outside the tunnel (inactive).

We define the rate of change in the number of ants in the tunnel as the number of ants entering minus the number of ants leaving. We assume that a fraction (c_1) of N total ants are trying to enter the tunnel of fixed length L at any given time. We also assume that ants leave the tunnel at a rate proportional to the probability of finding the tunnel blocked in a given traversal. This assumption corresponds to the crowding-induced inactivity which is incorporated into the cellular automata. Thus, we define the rate of change of active ants in the system as:

$$\frac{dn}{dt} = c_1 N - c_2 P_f \quad (2)$$

where c_1 and c_2 are constants, and P_f is the probability that an ant encounters a blockage during tunnel traversal (and thus, denotes a failed pellet excavation). We assume that the tunnel is excavated very slowly relative to ant movements, and thus the tunnel length, L , can be treated as constant at any point in time. This simplification also ignores the time delay between an ant choosing to leave the tunnel and doing so.

An ant successfully traverses the tunnel if it is able to reach the other side without running into a blockade. Because the tunnel is two body widths wide, we can say that the tunnel is blocked at a specific location if there are two ants across the width of the tunnel at that location (as shown in Fig. 7 at time t_i). We assume an area of $2L$ (twice the tunnel length) with n active ants randomly distributed throughout the tunnel. We find that the probability of a blockage occurring at any given location in the tunnel, at a single instance in time, scales quadratically with the density of ants in the tunnel:

$$P_b = \frac{n(n-1)}{2L(2L-1)} \approx \frac{n^2}{4L^2} \quad (3)$$

As an ant moves through the tunnel to excavate a grain and then deposit, it must move a total distance $2L$, with a probability of finding a blockade at every step. Because other ants also move every step, we assume that the probability of a blockade is history independent (ants randomly redistribute each step). This simplification ignores ant interactions - ants moving systematically could affect these probabilities conditionally. With this assumption, the probability of successfully traversing the tunnel is:

$$P_s = (1 - P_b)^{2L} \approx 1 - 2LP_b \approx 1 - \frac{n^2}{2L} \quad (4)$$

The above uses the binomial approximation, which assumes $\frac{n^2}{L^2} \ll 1$. Therefore, the probability of an ant experiencing a blockage at any point during a tunnel traversal is:

$$P_f = 2LP_b \approx \frac{n^2}{2L} \quad (5)$$

Substituting this into Equation 2, we find:

$$\frac{dn}{dt} = c_1N - c_2\frac{n^2}{2L} \quad (6)$$

Here, we treat the length of the tunnel as roughly constant relative to the changes in the numbers of ants and fold $2L$ into c_2 . We note that in experiment, we observe an increase in activity at the onset of digging, followed by a decay to a steady state over long times (see Figures 4-5). At the peak of activity and after a long time, we observe that $\frac{dn}{dt} = 0$. Using this condition, we find that the model predicts experimental scaling observations:

$$n \propto \sqrt{N} \quad (7)$$

2) *Optimality of excavation rates:* We posit that ants attempt to maximize the speed of digging. The rate of digging is proportional the number of ants traversing the tunnel, which is equal to the number of active ants multiplied by their probability of successful traversal:

$$D = nP_s = n\left(1 - \frac{n^2}{2L}\right) \quad (8)$$

Where D is the rate of deposits and P_s is the probability of a successful traversal. To find the number of active ants, n , that would maximize D , we differentiate D with respect to n and find its roots:

$$\frac{dD}{dn} = 1 - c\frac{n^2}{2L} = 0 \quad (9)$$

Evaluating, we find:

$$n \propto \sqrt{L} \quad (10)$$

The number of active ants required to maximize digging is proportional to \sqrt{L} . From Equation 7 and experimental results, we observe that the number of active ants scales with \sqrt{N} . This means that the ants would maximize digging rates in a scenario where the length of the tunnel scaled with the total number of ants, or

$$N \propto L \quad (11)$$

In other words, ants' observed behaviors would optimize digging speeds if tunnel length was directly proportional to the number of ants. Observing this scaling law directly in experiment would be difficult. As ants dig tunnels, the lengths of the tunnels change, which in turn impacts the optimal group size.

Additionally, large numbers of ants do not dig a single tunnel - instead, ants are distributed across a nest, digging tunnels simultaneously. In these scenarios, defining the group size for a single tunnel becomes difficult. Nevertheless, it has been observed that the size of a group of ants is positively correlated with both the size and complexity of an ant nest and the length and speed of digging [39], [58], [59]. Also, a smaller group of ants will stop digging a tunnel earlier than a larger group [60]. Therefore, in natural environments where ants have already begun to dig tunnels, ants that are part of larger colonies would naturally be digging in larger tunnels. If this correlation is linear, the behavior observed in this study would indeed optimize for digging speed.

III. DISCUSSION

Collectives often utilize division of labor to accomplish goals in constrained environments. Here, we analyze one collective system, tunnel construction in *S invicta* fire ants, through experiments, simulation, and theoretical modeling to observe the emergence of unequal workloads as numbers of workers rise. We also find that the correlation between group size and inequality can be described by a simple scaling law: the number of ants actively contributing to digging is approximately equal to the square root of the total group size. This finding parallels generalized scaling laws which have been observed in other social systems which previously lacked mechanistic explanations. The CA simulation and theoretical model used in this work both suggest that local cues, such as the levels of confinement or encounter rate, may drive decision making at the individual level, and thus result in the scaling of workload inequality observed in the collective. Specifically, we suggest that if individuals choose to remain inactive in crowded conditions, a quadratic failure rate emerges which results in a square root scaling in participation rate. This result represents one of the first mechanistic explanations for the relationship between workload inequality and group size in collective systems.

The square root scaling law introduced in this work resembles scaling laws from other domains, which suggest that in large groups, only a small fraction of the group is responsible for a large portion of productive output. For example, in the late 19th century, Pareto observed that in economics, approximately 80% of wealth was concentrated in about 20% of a population, becoming the basis for the modern “Pareto Principle” [61]. Similarly, Price showed that this extreme inequality increased with group size; in observations of scientific publishing, Price demonstrated that roughly the square root of the total authors were responsible for one half of all published papers [62]. The linguist Zipf showed that in the written language, a word’s frequency is inversely proportional to its rank [63], an observation which has been shown to extend to city populations and income distributions [64], [65].

However, studies of Price’s and Zipf’s laws are largely observational and cannot point to a specific

causal mechanism. The principles underlying these scaling laws for inequality, in both human societies and other biological collectives, remain unclear. In this study, we provide an explanation involving the rate of blockages in the tunnel - this corresponds to a failure rate proportional to n^2 , which results in the square root scaling. Interestingly, particle collisions in a fixed volume also scale quadratically with population density. This may point towards similar scaling laws in other constrained biological collectives where collisions strongly influence dynamics, such as within honeybee nests or ant rafts. However, we believe that these trends may not hold for *S. invicta* ants at higher populations - at colony sizes, ants would not only dig one tunnel. Instead, we expect that ants would dig many tunnels in parallel, as we observe in nature. Further work is needed to understand how these patterns of workload inequality emerge in tasks which are differently constrained.

Importantly, our modeling shows that these global changes can emerge via local interactions: the quadratic failure rate in our theoretical model emerges if individuals choose to exit the tunnel when they are “blocked.” Similarly, the CA model relies on individuals making decisions based on their rate of successful movement in the tunnel. Only when this individual decision making is introduced into the CA is the simulation able to accurately capture the square root scaling relationship. Thus, both models suggest that local information drives individual decision making, and thus results in rates of emergent inequality observed in the collective. This idea bears some similarities to Response Threshold Models (RTMs), which suggest that workers are active only when external stimuli exceed internal thresholds [66]–[68]. Variable thresholds allow for thresholds to change over time based on external factors [49], such as how many times the task has been performed [69], [70]. The CA model explored in this work bears some similarity to variable response threshold models, in that an ant’s intrinsic work-rest ratio is fixed, but the rate of engagement with the task is modulated by external factors.

The adaptive function of workload inequality in overall collective success is still not universally agreed upon. Using CA simulations, Aguilar et al. suggest that a $G \approx 0.75$ within the tunnel corresponds with optimal traffic flow and fastest digging speeds (using their formulation for Gini coefficient). However, this Gini coefficient was optimal only for a group size of 30 ants: another CA simulation with 60 ants showed that their optimal Gini coefficient increased to ≈ 0.8 . The present study echoes the idea that optimal participation rates likely vary with the group size. In our theoretical analysis, we suggest that the changes in participation rates observed (namely, the square root scaling) would optimize digging speeds if the group size was proportional to the length of the tunnels. This analysis provides a path towards understanding how decision making at the individual level can allow a group to maintain high performance in the presence of variable environmental constraints.

However, our mechanistic analysis relies on the assumption that spatial constraints are the primary

driver of group dynamics. In tasks with different constraints, many other explanations are possible to describe the adaptive function of workload inequality [71]. Some subset of studies argue that maintaining a “reserve” of inactive ants allows the colony to continue to function when active workers inevitably stop working [48]. Others suggest that the colony produces “extra” workers, choosing only to employ the only most efficient workers of any given group to optimize performance [72]. Some argue that under certain conditions, inequality may simply be a byproduct of the task allocation process, without necessarily serving an adaptive function [50]. Future studies may seek to explore the functional advantages of workload inequality across a variety of tasks within a colony. Certainly, under the presence of environmental constraints, choosing to employ the optimal subset of individuals may prevent deleterious clogs and traffic jams, ultimately aiding collective success.

Finally, the workload scaling observations derived in this work were made possible by a new method for monitoring activity in ants. This methodology allows for automatic tracking of total workload via counting trips to/from an excavation site. While we focus specifically on fire ant digging in this paper, this method could be employed to study workload distributions in any social insect collective for which a task involves repeated trips to a singular site. The automatic tracking algorithm employed in this work was capable of analyzing 20 hours of video data, and subsequently calculating workload and activity information, in minutes. In prior work, counting individual contributions had often been done manually, requiring additional labor and reducing the amount of usable data [4], [54]. The method introduced in this study represents a major step towards enabling more rapid monitoring and analysis of workload inequality in social insects. However, this method remains untested for groups larger than 10 ants— in these cases, we anticipate that using more advanced software may be required to accurately monitor behavior.

IV. MATERIALS AND METHODS

A. Details of custom MATLAB algorithm for ant tracking

For trials with 10 or fewer ants, individual ant locations were tracked via an algorithm which performed color thresholding and isolated connected components, or groups of adjacent pixels. The largest connected components within each pre-identified color range (corresponding to color markings on ant gasters) were isolated. For each connected component, we computed both the size of the connected region, and the distance of each connected region to its location in the prior frame. We computed a weighted sum of these two parameters (size of region and distance to prior location). The weights were chosen via manual trial and error to maximize tracking accuracy. For each color, we then chose the connected region with the maximum weighted sum. These regions were presumed to belong to individual ants of each color code and were used to assign the pixel location of each ant. If a particular ant was not identified within the camera region, its location was assigned as either inside the tunnel, or at the camera boundary if the ant was near a boundary in a prior frame.

B. Details of CA simulation

The cellular automata simulation used in this work was built in MATLAB and was run using MATLAB's Parallel Computing Toolbox to accelerate simulation times. The simulation relied on an agent-based model based on prior work by William Savoie [4] that was built upon a tunnel whose cells can take on various states: unexcavated (filled with sand), excavated, empty (no sand), or containing a single ant. Each ant in the simulation can have one of five activity states: moving in tunnel (ascending), moving in tunnel (descending), digging, depositing a pellet, or resting (waiting for $P > e^{-1/(IC_0)P_0}$). The simulated "tunnel" is comprised of cells which are one ant body width wide and one ant body width long (accommodating a single ant at any given time). The simulated tunnel is two cells wide and 100 cells long. At the simulation times explored in this work, this length is sufficient to guarantee that no group of simulated ants will dig the full length of the tunnel. We assume that ants travel one cell in either direction per timestep. Using estimations of ant walking speed from prior literature as 0.27 body lengths per second [54], we approximate the real-world time of a single simulation timestep as 3.7 seconds (equivalent to the time it takes an ant to travel a single body length). Ants in the tunnel move laterally with probability 0.52 and reverse with a probability 0.34 when blocked by ants below them.

We utilize results from prior literature to estimate the number of ant trips which resulted in a single cell being removed from the end of the tunnel (representing tunnel excavation). We found that it takes 206 trips per cm of excavation [54], or 40 trips per cell excavated, assuming two cells must be excavated

for a full row of cells to be removed from the tunnel. Similarly, observations from prior work revealed that ants spend an average of 8.5 seconds excavating [54], which we approximate as 2 simulation timesteps. All parameters used in the CA simulation are shown in Table I (Supplemental Information). Results from a single CA simulation trial, including ant activity, excavation rates, and Lorenz curves, are shown in Figure 11 (Supplemental Information).

C. Estimating excavation rates across all experimental trials

To estimate excavation rates from all experimental data, we assume that excavation rates scale roughly linearly with the number of ants which engage in digging, as observed in [39]. We record the number of pellets transported during each hour of every experimental trial. We also record the number of ants who transport any number of pellets during each of those hour-long periods, denoting this quantity as the number of “active ants” in each period. We then plot pellets deposited in each hour vs. the number of active ants in each hour (shown in Figure 12A in the Supplemental Information). The hourly excavation rates across experimental trials are highly variable. We then fit a line to this data via least squares regression. The resultant fit rate is ≈ 9.5 pellets per active ant per hour of digging (shown in Figure 12A). This excavation rate represents a rough proxy for the number of pellets excavated by a single ant in one hour. For comparison, we examine the hour in which the most pellets were excavated in each trial. These data points are represented in Figure 12B in the Supplemental Information. In this case, the excavation rate for the hours of maximum activity is 13.8 pellets per active ant per hour.

D. Calculating excavation rates in CA simulation data

To estimate excavation rates for simulation trials, we use a similar procedure to the one used to calculate experimental excavation rates. For all 10 iterations run at each set of simulation parameters, we record the number of pellets transported during each hour. We also record the number of ants that transport at least one pellet during each of those hour-long periods. This results in a total of 880 hours for each set of parameters (8 hours in each simulation x 10 iterations x 11 different group sizes tested for each set of parameters). Fitting a line via least squares regression to this data for a single set of parameters ($C_0 = 10$, $R = 0.1$, $\tau_0 = 10$, $\tau_s = 2$) yields a resultant fit rate of ≈ 8.1 pellets per active ant per hour (Figure 13A in the Supplemental Information). We also analyze the rates if the total number of pellets transported at the end of each 8 hour trial is used for calculation instead. We compare total pellets transported to mean number of active ants over eight hours (Figure 13B in the Supplemental Information). The excavation rate estimated from a linear fit to these 110 trials is the same as that for

all hours of simulation (for the same set of simulation parameters), and thus we use this simplified form of the calculation for reporting simulation excavation rates for each set of parameters.

V. REFERENCES

- [1] C. W. Reynolds, "Flocks, herds and schools: A distributed behavioral model," in *Proceedings of the 14th annual conference on Computer graphics and interactive techniques*, 1987, pp. 25–34.
- [2] I. D. Couzin, J. Krause *et al.*, "Self-organization and collective behavior in vertebrates," *Advances in the Study of Behavior*, vol. 32, no. 1, pp. 10–1016, 2003.
- [3] M. Moussaid, S. Garnier, G. Theraulaz, and D. Helbing, "Collective information processing and pattern formation in swarms, flocks, and crowds," *Topics in Cognitive Science*, vol. 1, no. 3, pp. 469–497, 2009.
- [4] J. Aguilar, D. Monaenkova, V. Linevich, W. Savoie, B. Dutta, H.-S. Kuan, M. D. Betterton, M. A. D. Goodisman, and D. I. Goldman, "Collective clog control: Optimizing traffic flow in confined biological and robophysical excavation," *Science*, vol. 361, no. 6403, pp. 672–677, 2018.
- [5] C. Detrain and J.-L. Deneubourg, "Self-organized structures in a superorganism: do ants "behave" like molecules?" *Physics of Life Reviews*, vol. 3, no. 3, pp. 162–187, 2006.
- [6] D. M. Gordon, "From division of labor to the collective behavior of social insects," *Behavioral ecology and sociobiology*, vol. 70, no. 7, pp. 1101–1108, 2016.
- [7] G. E. Robinson, "Division of labor in insect societies," *Encyclopedia of insects*, pp. 297–299, 2009.
- [8] R. Jeanson, "Within-individual behavioural variability and division of labour in social insects," *Journal of Experimental Biology*, vol. 222, no. 10, p. jeb190868, 2019.
- [9] G. F. Oster and E. O. Wilson, *Caste and Ecology in the Social Insects*. Princeton University Press, 1978.
- [10] S. N. Beshers and J. H. Fewell, "Models of division of labor in social insects," *Annual Review of Entomology*, vol. 46, no. Volume 46, 2001, pp. 413–440, 2001.
- [11] C. T. Holbrook, P. M. Barden, and J. H. Fewell, "Division of labor increases with colony size in the harvester ant *Pogonomyrmex californicus*," *Behavioral Ecology*, vol. 22, no. 5, pp. 960–966, 2011.
- [12] D. Charbonneau, N. Hillis, and A. Dornhaus, "'Lazy' in nature: ant colony time budgets show high 'inactivity' in the field as well as in the lab," *Insectes Sociaux*, vol. 62, no. 1, pp. 31–35, 2015.
- [13] A. L. Toth and G. E. Robinson, "Worker nutrition and division of labour in honeybees," *Animal behaviour*, vol. 69, no. 2, pp. 427–435, 2005.
- [14] Z.-Y. Huang and G. E. Robinson, "Honeybee colony integration: worker-worker interactions mediate hormonally regulated plasticity in division of labor." *Proceedings of the National Academy of Sciences*, vol. 89, no. 24, pp. 11 726–11 729, 1992.
- [15] S. A. West, R. M. Fisher, A. Gardner, and E. T. Kiers, "Major evolutionary transitions in individuality," *Proceedings of the National Academy of Sciences*, vol. 112, no. 33, pp. 10 112–10 119, 2015.
- [16] D. C. Queller and J. E. Strassmann, "Kin Selection and Social Insects," *BioScience*, vol. 48, no. 3, pp. 165–175, 1998.
- [17] E. O. Wilson, "Social Insects," *Science*, vol. 172, no. 3981, pp. 406–406, 1971.
- [18] J. E. Strassmann and D. C. Queller, "Insect societies as divided organisms: The complexities of purpose and cross-purpose," *Proceedings of the National Academy of Sciences*, vol. 104, no. suppl_1, pp. 8619–8626, 2007.
- [19] E. O. Wilson, *Success and Dominance in Ecosystems: The Case of the Social Insects*. Ecology Institute, 1990.
- [20] A. F. G. Bourke and N. R. Franks, *Social Evolution in Ants*. Princeton University Press, 1995.
- [21] D. Charbonneau and A. Dornhaus, "When doing nothing is something. How task allocation strategies compromise between flexibility, efficiency, and inactive agents," *Journal of Bioeconomics*, vol. 17, no. 3, pp. 217–242, 2015.
- [22] M. G. Smith and C. Riehl, "Workload Distribution and Division of Labor in Cooperative Societies," *The Quarterly Review of Biology*, vol. 97, no. 3, pp. 183–210, 2022.
- [23] E. Invernizzi and G. D. Ruxton, "Deconstructing collective building in social insects: implications for ecological adaptation and evolution," *Insectes Sociaux*, vol. 66, no. 4, pp. 507–518, 2019.

- [24] D. M. Gordon, “The Ecology of Collective Behavior in Ants,” *Annual Review of Entomology*, vol. 64, no. Volume 64, 2019, pp. 35–50, 2019.
- [25] J. W. Wenzel, “14. Evolution of Nest Architecture,” in *The Social Biology of Wasps*, K. G. Ross and R. W. Matthews, Eds. Cornell University Press, 1991, pp. 480–519.
- [26] G. Theraulaz, E. Bonabeau, and J.-L. Deneubourg, “The origin of nest complexity in social insects,” *Complexity*, vol. 3, no. 6, pp. 15–25, 1998.
- [27] M. H. Hansell, *Animal Architecture*. OUP Oxford, 2005.
- [28] G. Theraulaz, J. Gautrais, S. Camazine, and J.-L. Deneubourg, “The formation of spatial patterns in social insects: from simple behaviours to complex structures,” *Philosophical Transactions of the Royal Society of London. Series A: Mathematical, Physical and Engineering Sciences*, vol. 361, no. 1807, pp. 1263–1282, 2003.
- [29] S. Camazine, J.-L. Deneubourg, N. R. Franks, J. Sneyd, G. Theraulaz, and E. Bonabeau, *Self-Organization in Biological Systems*. Princeton University Press, 2020.
- [30] A. Perna and G. Theraulaz, “When social behaviour is moulded in clay: on growth and form of social insect nests,” *Journal of Experimental Biology*, vol. 220, no. 1, pp. 83–91, 2017.
- [31] M. W. Moffett, S. Garnier, K. M. Eisenhardt, N. R. Furr, M. Warglien, C. Sartoris, W. Ocasio, T. Knudsen, L. A. Bach, and J. Offenberg, “Ant colonies: building complex organizations with minuscule brains and no leaders,” *Journal of Organization Design*, vol. 10, no. 1, pp. 55–74, 2021.
- [32] D. Sumpter, “The principles of collective animal behaviour,” *Philosophical Transactions of the Royal Society B: Biological Sciences*, vol. 361, no. 1465, pp. 5–22, 2005.
- [33] J. H. Fewell, “Social Insect Networks,” *Science*, vol. 301, no. 5641, pp. 1867–1870, 2003.
- [34] I. D. Couzin, “Collective cognition in animal groups,” *Trends in Cognitive Sciences*, vol. 13, no. 1, pp. 36–43, 2009.
- [35] P. M. Bardunias and N.-Y. Su, “Queue Size Determines the Width of Tunnels in the Formosan Subterranean Termite (Isoptera: Rhinotermitidae),” *Journal of Insect Behavior*, vol. 23, no. 3, pp. 189–204, 2010.
- [36] A. Khuong, J. Gautrais, A. Perna, C. Sbaï, M. Combe, P. Kuntz, C. Jost, and G. Theraulaz, “Stigmergic construction and topochemical information shape ant nest architecture,” *Proceedings of the National Academy of Sciences*, vol. 113, no. 5, pp. 1303–1308, 2016.
- [37] W. R. Tschinkel, *The Fire Ants*. Harvard University Press, 2013.
- [38] D. Cassill, W. Tschinkel, and S. Vinson, “Nest complexity, group size and brood rearing in the fire ant, *Solenopsis invicta*,” *Insectes Sociaux*, vol. 49, no. 2, pp. 158–163, 2002.
- [39] N. Gravish, M. Garcia, N. Mazouchova, L. Levy, P. B. Umbanhowar, M. A. D. Goodisman, and D. I. Goldman, “Effects of worker size on the dynamics of fire ant tunnel construction,” *Journal of The Royal Society Interface*, vol. 9, no. 77, pp. 3312–3322, 2012.
- [40] N. Gravish, D. Monaenkova, M. A. D. Goodisman, and D. I. Goldman, “Climbing, falling, and jamming during ant locomotion in confined environments,” *Proceedings of the National Academy of Sciences*, vol. 110, no. 24, pp. 9746–9751, 2013.
- [41] N. Gravish, G. Gold, A. Zangwill, M. A. D. Goodisman, and D. I. Goldman, “Glass-like dynamics in confined and congested ant traffic,” *Soft Matter*, vol. 11, no. 33, pp. 6552–6561, 2015.
- [42] B. Hölldobler and E. O. Wilson, *The Ants*. Harvard University Press, 1990.
- [43] R. Scheiner and G. Bloch, “Editorial overview: How do social insects know their tasks?” *Current Opinion in Insect Science*, vol. 66, p. 101257, 2024.
- [44] A. Duarte, F. J. Weissing, I. Pen, and L. Keller, “An Evolutionary Perspective on Self-Organized Division of Labor in Social Insects,” *Annual Review of Ecology, Evolution, and Systematics*, vol. 42, no. Volume 42, 2011, pp. 91–110, 2011.
- [45] S. N. Beshers, “Regulation of division of labor in insects: a colony-level perspective,” *Current Opinion in Insect Science*, vol. 61, p. 101155, 2024.
- [46] D. Charbonneau and A. Dornhaus, “Workers ‘specialized’ on inactivity: Behavioral consistency of inactive workers and their role in task allocation,” *Behavioral Ecology and Sociobiology*, vol. 69, no. 9, pp. 1459–1472, 2015.

- [47] E. Hasegawa, Y. Ishii, K. Tada, K. Kobayashi, and J. Yoshimura, "Lazy workers are necessary for long-term sustainability in insect societies," *Scientific Reports*, vol. 6, no. 1, p. 20846, 2016.
- [48] D. Charbonneau, T. Sasaki, and A. Dornhaus, "Who needs 'lazy' workers? Inactive workers act as a 'reserve' labor force replacing active workers, but inactive workers are not replaced when they are removed," *PLOS ONE*, vol. 12, no. 9, p. e0184074, 2017.
- [49] T. Feng, D. Charbonneau, Z. Qiu, and Y. Kang, "Dynamics of task allocation in social insect colonies: scaling effects of colony size versus work activities," *Journal of Mathematical Biology*, vol. 82, no. 5, p. 42, 2021.
- [50] M. Khajehnejad, J. García, and B. Meyer, "Explaining workers' inactivity in social colonies from first principles," *Journal of The Royal Society Interface*, vol. 20, no. 198, p. 20220808, 2023.
- [51] M. Porfiri, N. Abaid, and S. Garnier, "Socially driven negative feedback regulates activity and energy use in ant colonies," *PLoS computational biology*, vol. 20, no. 11, p. e1012623, 2024.
- [52] M. Napoli, R. Sipahi, and M. Porfiri, "The role of colony size on activity rhythms of ants," *Journal of Theoretical Biology*, p. 112286, 2025.
- [53] W. R. Tschinkel, "Ant architecture: the wonder, beauty, and science of underground nests," in *Ant Architecture*. Princeton University Press, 2021.
- [54] R. Avinery, K. O. Aina, C. J. Dyson, H.-S. Kuan, M. D. Betterton, M. A. D. Goodisman, and D. I. Goldman, "Agitated ants: regulation and self-organization of incipient nest excavation via collisional cues," *Journal of The Royal Society Interface*, vol. 20, no. 202, p. 20220597, 2023.
- [55] J. H. Fewell and J. F. Harrison, "Scaling of work and energy use in social insect colonies," *Behavioral Ecology and Sociobiology*, vol. 70, no. 7, pp. 1047–1061, 2016.
- [56] K. O. Aina, R. Avinery, H.-S. Kuan, M. D. Betterton, M. A. D. Goodisman, and D. I. Goldman, "Toward Task Capable Active Matter: Learning to Avoid Clogging in Confined Collectives via Collisions," *Frontiers in Physics*, vol. 10, 2022.
- [57] J. D. Murray, *Mathematical Biology I. An Introduction*. Springer New York, NY, 2002.
- [58] P. Rasse and J. Deneubourg, "Dynamics of nest excavation and nest size regulation of *Lasius niger* (hymenoptera: Formicidae)," *Journal of Insect Behavior*, vol. 14, pp. 433–449, 2001.
- [59] C. Buhl, J. Gautrais, J.-L. Deneubourg, and G. Theraulaz, "Nest excavation in ants: group size effects on the size and structure of tunneling networks," *Naturwissenschaften*, vol. 91, no. 12, pp. 602–606, 2004.
- [60] A. Bruce, A. Pérez-Escudero, T. Czaczkes, and M. Burd, "The digging dynamics of ant tunnels: movement, encounters, and nest space," *Insectes Sociaux*, vol. 66, no. 1, pp. 119–127, 2019.
- [61] R. Sanders, "The pareto principle: its use and abuse," *Journal of Services Marketing*, vol. 1, no. 2, pp. 37–40, 1987.
- [62] D. J. D. S. Price, *Little science, big science*. Columbia university press, 1963.
- [63] G. K. Zipf, "Selected studies of the principle of relative frequency in language," 1932.
- [64] B. M. Hill, "The rank-frequency form of zipf's law," *Journal of the American Statistical Association*, vol. 69, no. 348, pp. 1017–1026, 1974.
- [65] R. E. Wyllys, "Empirical and theoretical bases of zipf's law," 1981.
- [66] R. Jeanson, J. H. Fewell, R. Gorelick, and S. M. Bertram, "Emergence of increased division of labor as a function of group size," *Behavioral Ecology and Sociobiology*, vol. 62, no. 2, pp. 289–298, 2007.
- [67] E. Bonabeau, G. Theraulaz, and J.-L. Deneubourg, "Fixed Response Thresholds and the Regulation of Division of Labor in Insect Societies," *Bulletin of Mathematical Biology*, vol. 60, no. 4, pp. 753–807, 1998.
- [68] G. E. Robinson and R. E. Page, "Genetic basis for division of labor in an insect society," in *The genetics of social evolution*. CRC Press, 2019, pp. 61–80.
- [69] J. Gautrais, G. Theraulaz, J.-L. Deneubourg, and C. Anderson, "Emergent polyethism as a consequence of increased colony size in insect societies," *Journal of theoretical biology*, vol. 215, no. 3, pp. 363–373, 2002.

- [70] G. Theraulaz, E. Bonabeau, and J. Deneubourg, “Response threshold reinforcements and division of labour in insect societies,” *Proceedings of the Royal Society of London. Series B: Biological Sciences*, vol. 265, no. 1393, pp. 327–332, 1998.
- [71] A. Dornhaus, J.-A. Holley, V. G. Pook, G. Worswick, and N. R. Franks, “Why do not all workers work? colony size and workload during emigrations in the ant *temnothorax albipennis*,” *Behavioral Ecology and Sociobiology*, vol. 63, no. 1, pp. 43–51, 2008.
- [72] A. Bernadou and R. Jeanson, “Randomness as a driver of inactivity in social groups,” *PLOS Computational Biology*, vol. 20, no. 12, p. e1012668, 2024.

VI. ACKNOWLEDGMENTS

We thank William Savoie for providing template code from his prior work [4], upon which we based the CA simulation used in this work. We also thank Ram Avinery for insightful guidance based on his prior work in CA modeling, particularly his model which similarly relied on an intrinsic work-rest ratio. We also thank various members of the Goodisman lab: namely, Paige Caine and Andrew Robertson, who assisted with ant husbandry throughout the time frame that the experiments were conducted. We also thank Prof. Takao Sasaki for providing advice on labeling and painting strategies for fire ants.

Funding: National Science Foundation Grant #NSF-IOS-2019799.

Author Contributions: Conceptualization: DIG, MADG, LKT, AR Methodology: LKT, AR Investigation: LKT, NW, AR Data curation: NN, NW, LKT Supervision: DIG, MADG Writing-original draft: LKT, AR Writing- review & editing: LKT, AR, DIG, MADG, NN, NW

Competing Interests: The authors declare that they have no competing interests.

Data and materials availability: All data are available in the main text or the supplementary materials. Additional code and/or data are available from the authors upon request.

VII. SUPPLEMENTAL INFORMATION

A. Summary of all experimental trials parsed via tracking algorithm

Here, we report the data collected for all experimental trials with 10 or fewer ants (Figures 14,15,16,17). Each row (A-D) represents a different trial and 20 hours of data are shown for each. All results shown here were generated via custom MATLAB tracking algorithms.

B. Results of full parameter sweeps in CA simulation

As denoted in Figure 9, only some model parameters have a measurable effect on resultant Gini coefficient trends. Here, we vary each parameter individually, and report the change in mean Gini coefficient for each combination of parameters. All results are shown in Figure 18A-D. Trends in excavation rates for all combinations of simulation parameters are shown in Figure 19.

Model parameters	Value / Range	Units	Source
Reversal probability	0.34		[4]
Tunnel width	2	cells	[4]
average time spent excavating	8.5	seconds	[54]
	2	timesteps	[54]
number of ant trips per cm excavated	206		[54]
number of ant trips per cell excavated	40		[54]
Cell width in CA simulation	1.1	mm	[39]
Cell length in CA simulation	3.95	mm	[39]
Average ant walking speed	0.27	BL/sec	[54]
Time per simulation timestep	3.70	sec	[54]
Total simulation time	8	hrs	
	7776	timesteps	
Lateral motion probability	0.52		[4]
time to drop pellet	10	seconds	[4]
	3	timesteps	[4]
R (default work/rest imbalance)	0.05 – 0.25		[54]
C_0 (crowding sensitivity parameter)	1 – 100		new
τ_0 (timescale for the tolerance of a work-to-rest imbalance)	1 – 100	timesteps	[54]
τ_s (period over which success rate is calculated)	1 – 10	timesteps	new

TABLE I: **Simulation Parameters.** All parameters used for implementation of the cellular automata are presented. We indicate the exact quantity if a single parameter value was used, or a range if multiple parameters were tested. Many parameter values were established in prior work, by either Aguilar et al. [4], Avinery et al. [54], or Gravish et al. [39]. Several new parameters are introduced in this CA model, and their values are indicated.

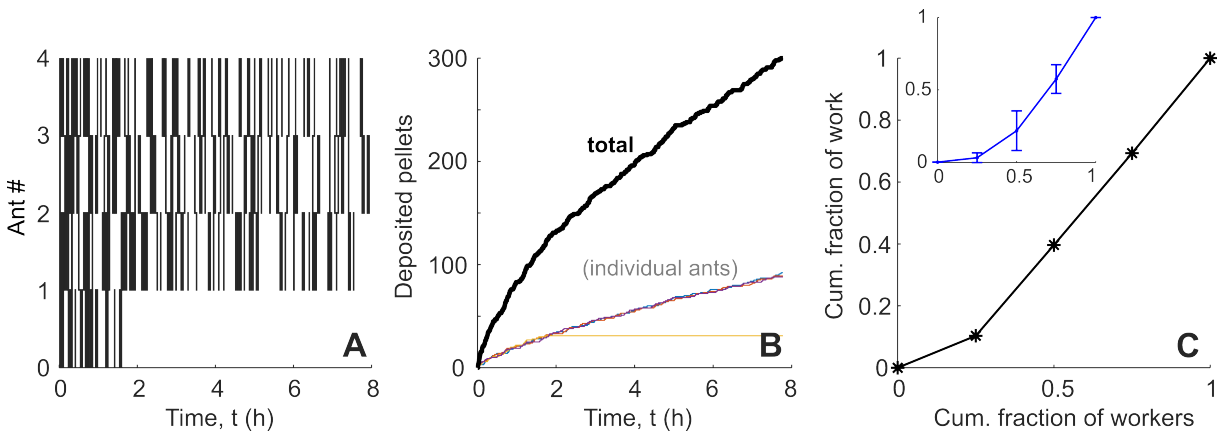


Fig. 11: **Single 4 ant trial simulation results.** (A) Plots of ant activity over the simulation duration, where a black dash indicates a grain transported at that time instance. Ants are sorted from highest to lowest activity (top to bottom). (B) Number of deposited pellets for each simulated ant, across the simulation duration. Colored lines represent individual ant contributions, while the black curve represents the total pellets deposited. (C) Lorenz curve, calculated from deposited pellets. Inset represents mean Lorenz curves across all 10 simulation trials for one set of simulation parameters ($R = 0.1$, $\tau_0 = 10$, $C_0 = 1$, $\tau_s = 2$).

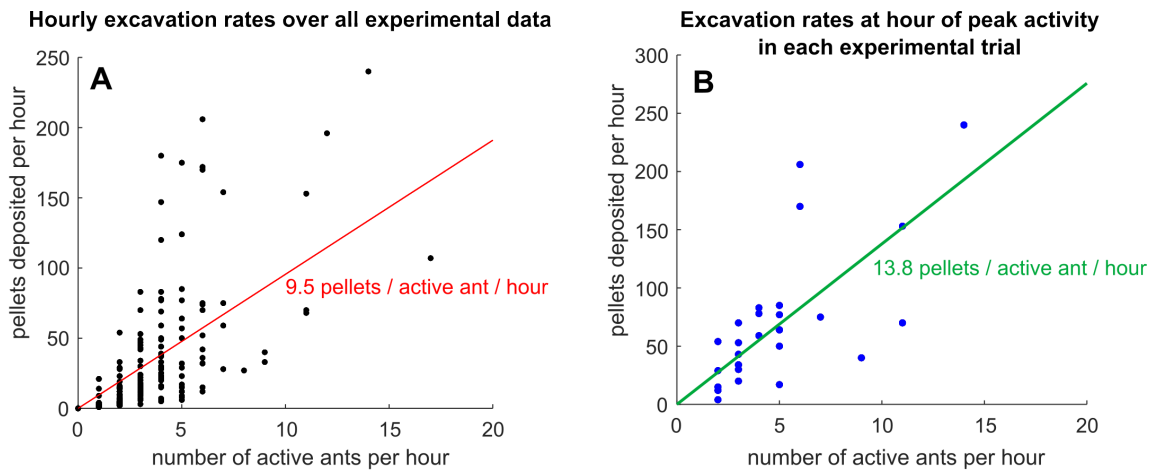


Fig. 12: **Method for calculating excavation rates in experimental trials** (A) The number of pellets deposited in each hour of experiment are plotted vs. the number of active ants in each hour of experiment. Red curve represents the line of best fit, with an effective mean excavation rate of 9.5 pellets/active ant/hour. (B) The number of pellets deposited in the most active hour of experiment are plotted vs. the number of active ants in each of these hours. The green curve represents the line of best fit, with an effective mean maximum excavation rate of 13.8 pellets/active ant/hour.

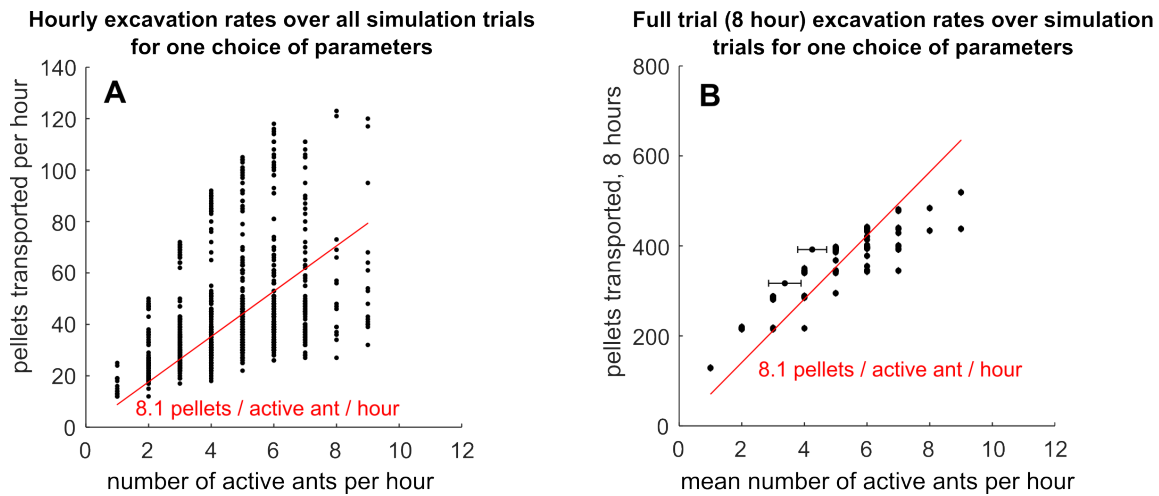


Fig. 13: **Method for calculating excavation rates in simulation trials** (A) The number of pellets deposited in each hour of simulation at one parameter combination ($C_0 = 10$, $R = 0.1$, $\tau_0 = 10$, $\tau_s = 2$) are plotted vs. the number of active ants in each hour. Red curve represents the line of best fit, with an effective mean excavation rate of 8.1 pellets/active ant/hour. (B) The number of pellets deposited over eight hours of simulation are plotted vs. the mean number of active ants across eight hours. Error bars represent standard deviation in number of active ants across all hours of the simulation. The red curve represents the line of best fit, with an effective mean excavation rate of 8.1 pellets/active ant/hour.

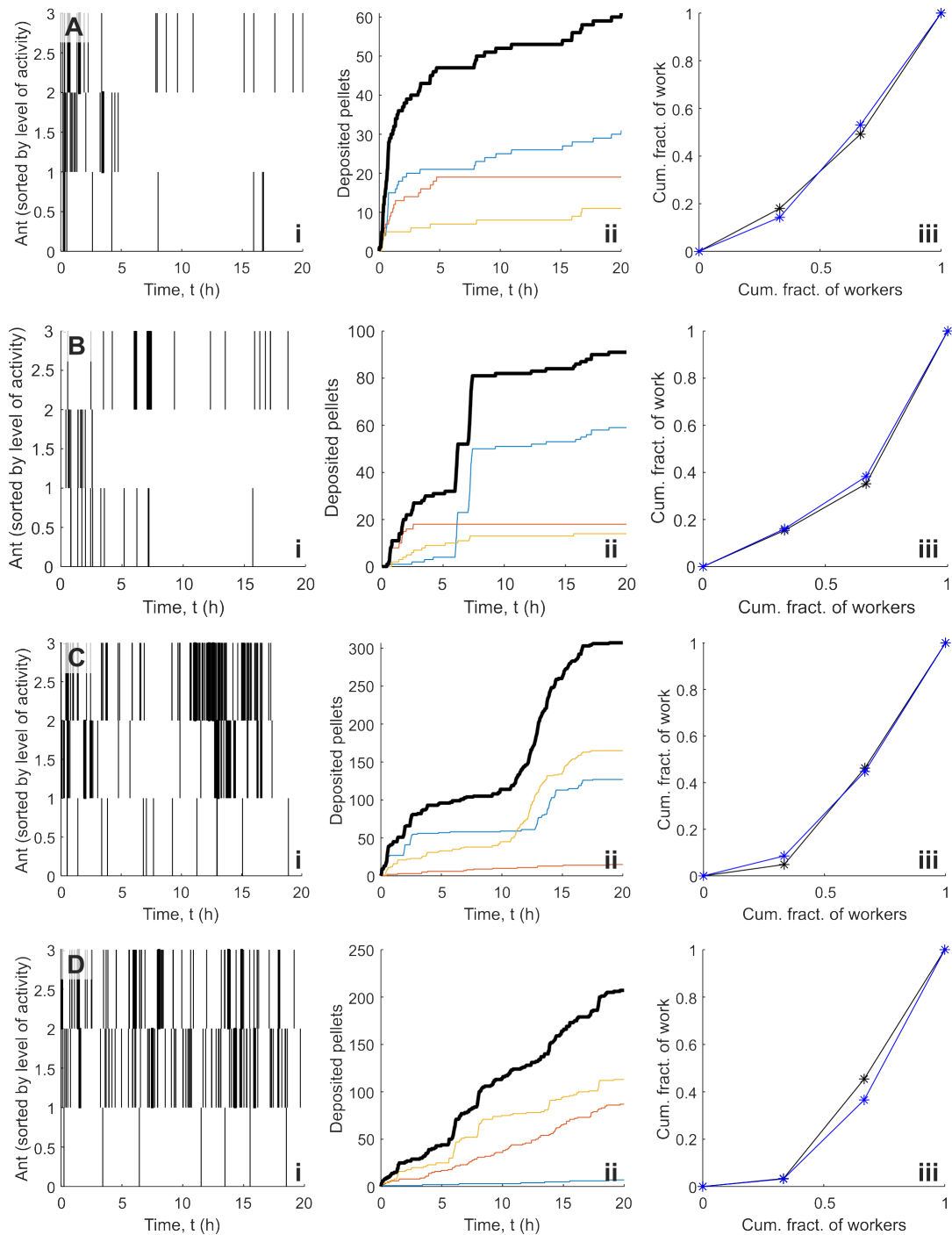


Fig. 14: **Experimental results, 3 ant trials.** Results for four different experimental trials, each containing three ants. Each row of plots (A-D) represents a single experimental trial. Leftmost plots (i) represent ant activity over the trial duration, where a black dash indicates a grain transported at that time instance. Each row corresponds to a different ant, with the top row corresponding to the most active ant. Center plots (ii) show the number of deposited pellets, as estimated by the tracking algorithm, for each ant across 20 hours. Colored lines represent individual ant contributions, while the black curve represents the total pellets deposited. Rightmost plots (iii) are Lorenz curves, representing cumulative fraction of grains moved, relative to cumulative fraction of workers involved, for the first 8 hours (blue) and full 20 hour trial (black).

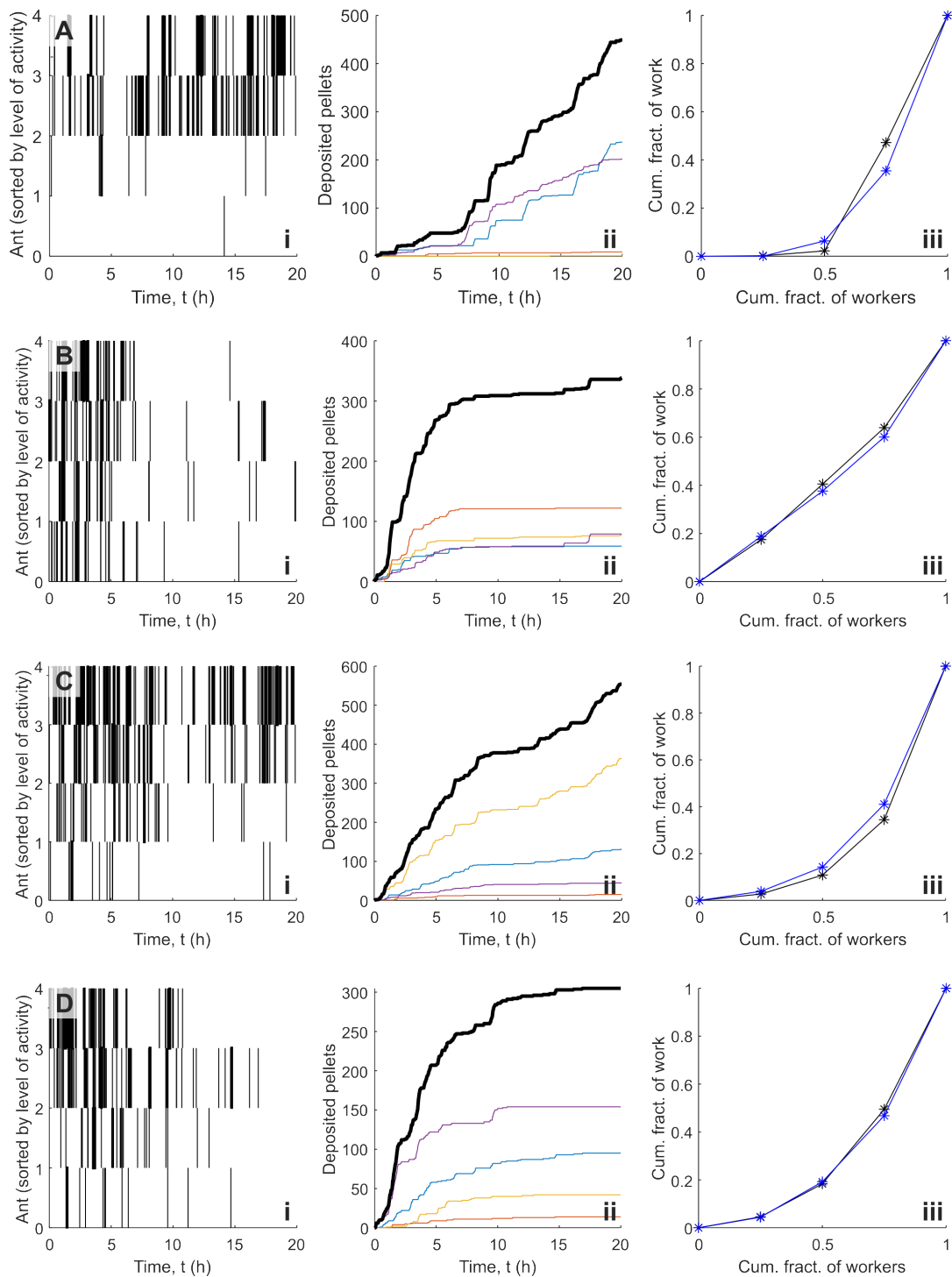


Fig. 15: **Experimental results, 4 ant trials.** Results for four different experimental trials, each containing four ants. Each row of plots (A-D) represents a single experimental trial. Leftmost plots (i) represent ant activity over the trial duration, where a black dash indicates a grain transported at that time instance. Each row corresponds to a different ant, with the top row corresponding to the most active ant. Center plots (ii) show the number of deposited pellets, as estimated by the tracking algorithm, for each ant across 20 hours. Colored lines represent individual ant contributions, while the black curve represents the total pellets deposited. Rightmost plots (iii) are Lorenz curves, representing cumulative fraction of grains moved, relative to cumulative fraction of workers involved, for the first 8 hours (blue) and full 20 hour trial (black).

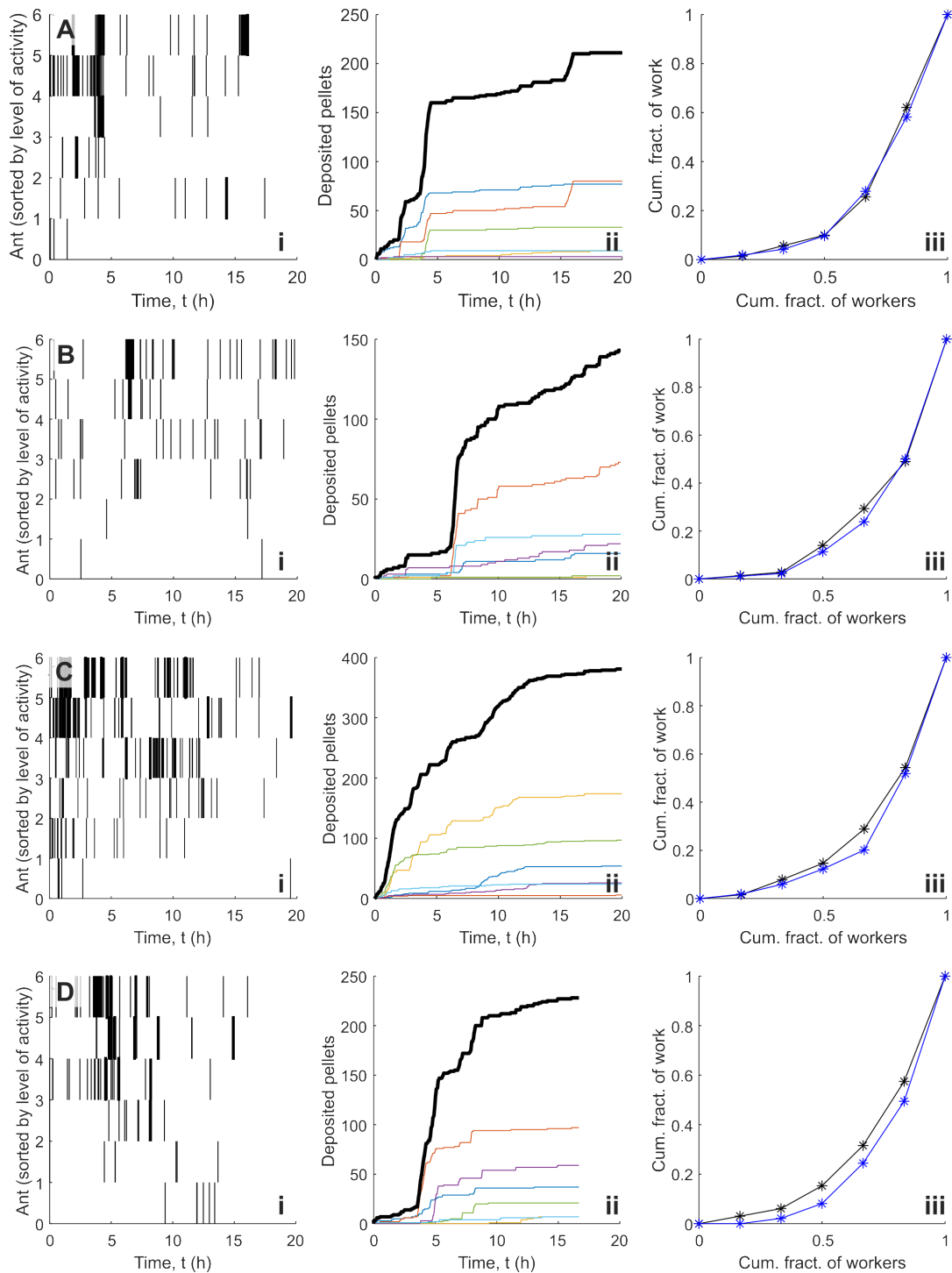


Fig. 16: **Experimental results, 6 ant trials.** Results for four different experimental trials, each containing six ants. Each row of plots (A-D) represents a single experimental trial. Leftmost plots (i) represent ant activity over the trial duration, where a black dash indicates a grain transported at that time instance. Each row corresponds to a different ant, with the top row corresponding to the most active ant. Center plots (ii) show the number of deposited pellets, as estimated by the tracking algorithm, for each ant across 20 hours. Colored lines represent individual ant contributions, while the black curve represents the total pellets deposited. Rightmost plots (iii) are Lorenz curves, representing cumulative fraction of grains moved, relative to cumulative fraction of workers involved, for the first 8 hours (blue) and full 20 hour trial (black).

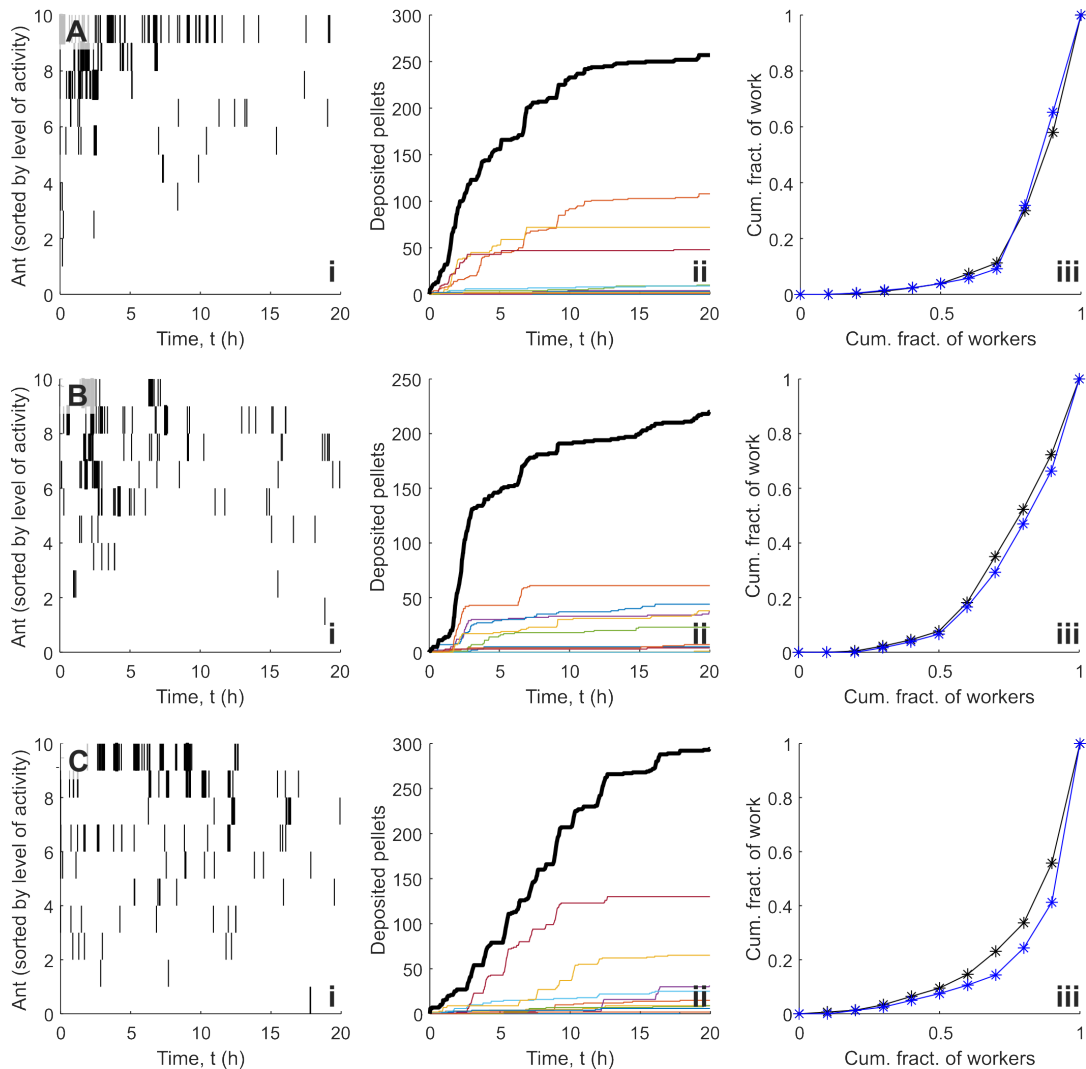


Fig. 17: **Experimental results, 10 ant trials.** Results for three different experimental trials, each containing ten ants. Each row of plots (A-C) represents a single experimental trial. Leftmost plots (i) represent ant activity over the trial duration, where a black dash indicates a grain transported at that time instance. Each row corresponds to a different ant, with the top row corresponding to the most active ant. Center plots (ii) show the number of deposited pellets, as estimated by the tracking algorithm, for each ant across 20 hours. Colored lines represent individual ant contributions, while the black curve represents the total pellets deposited. Rightmost plots (iii) are Lorenz curves, representing cumulative fraction of grains moved, relative to cumulative fraction of workers involved, for the first 8 hours (blue) and full 20 hour trial (black).

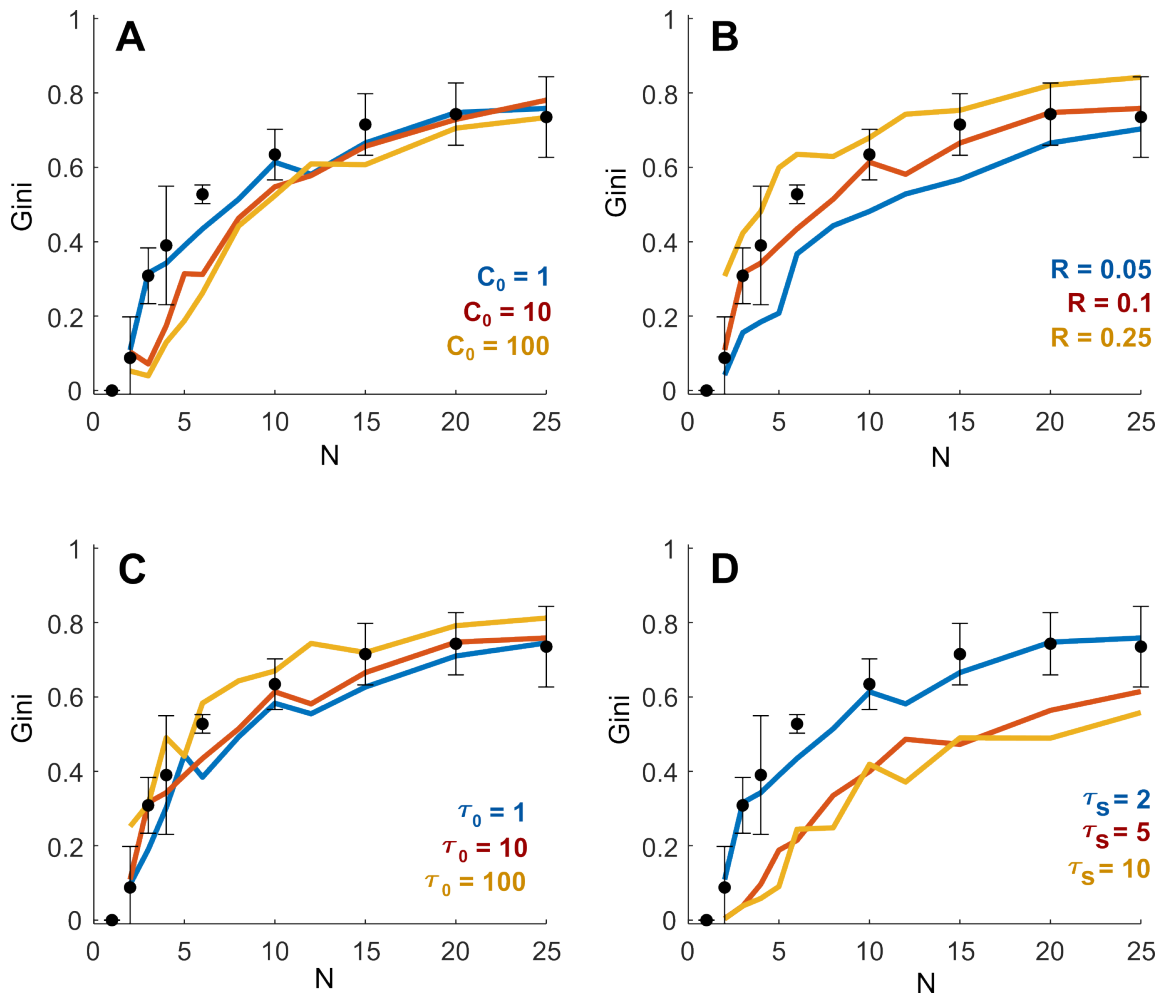


Fig. 18: **Effect of all parameters on CA simulation Gini coefficient estimates.** Each plot represents the effect of a single parameter on Gini coefficient trends; each line represents the mean Gini coefficients over 10 trials at each group size, N . In all plots (A)-(D), the default parameters are: $C_0 = 1$, $R = 0.1$, $\tau_0 = 10$, $\tau_s = 2$. **(A)** The effect of crowding sensitivity, C_0 . **(B)** The effect of intrinsic work-rest ratio, R . **(C)** The effect of timescale for the tolerance of a work-to-rest imbalance, τ_0 . **(D)** The effect of memory (timescale over which success rate is calculated), τ_s .

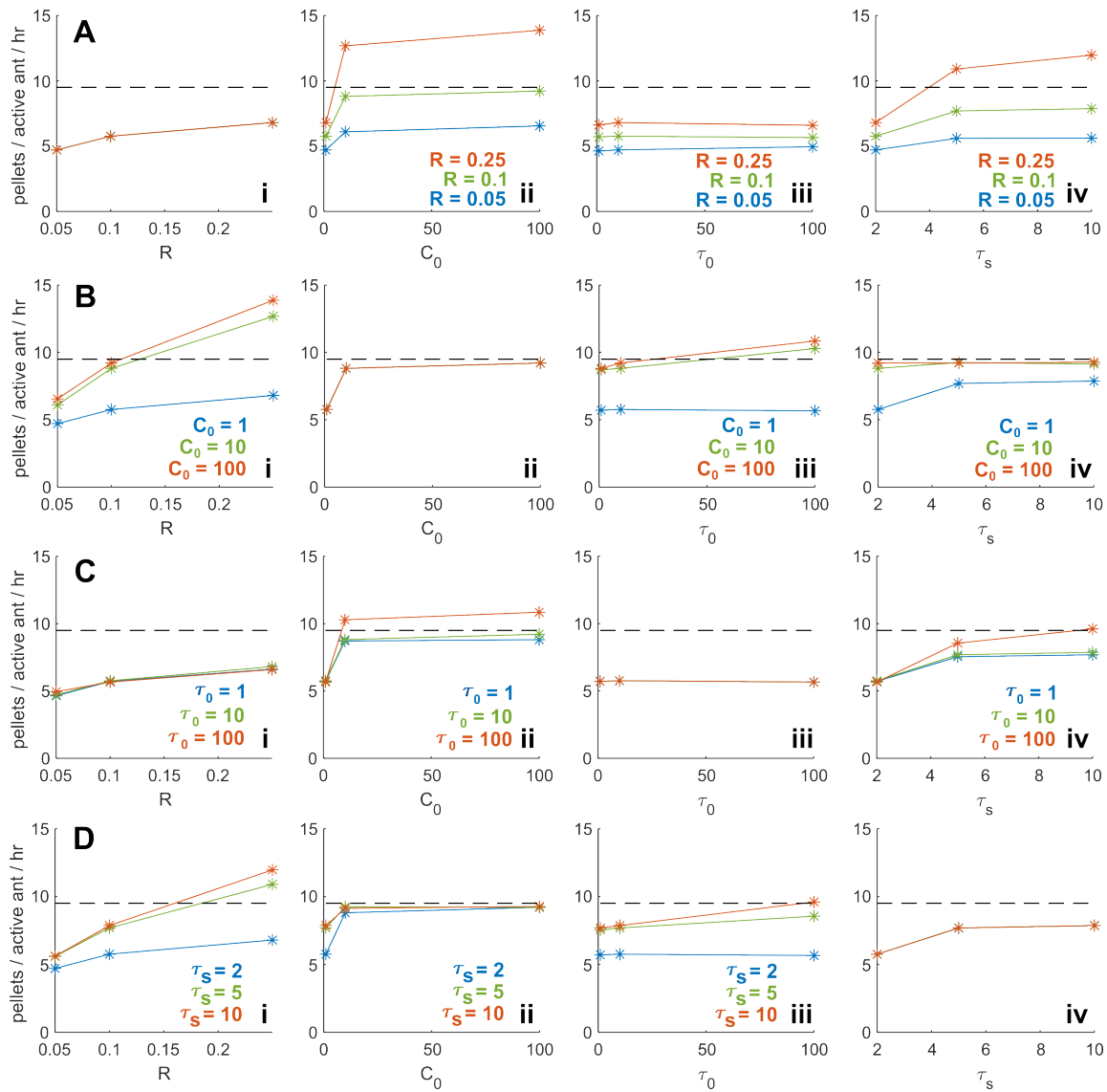


Fig. 19: **Effect of all parameters on CA simulation excavation rates.** Each plot (A-D) represents the effect of a single parameter on resultant excavation rates, and each subplot (i - iv) shows how varying another parameter affects these trends. Three values of each parameter were tested, and asterisks represent the estimated excavation rate for each parameter combination (based on the method described above). In all plots (A)-(D), unless otherwise indicated, the default parameters are: $C_0 = 1$, $R = 0.1$, $\tau_0 = 10$, $\tau_s = 2$. **(A)** The effect of intrinsic work-rest ratio, R . **(B)** The effect of crowding sensitivity, C_0 . **(C)** The effect of timescale for the tolerance of a work-to-rest imbalance, τ_0 . **(D)** The effect of memory (timescale over which success rate is calculated), τ_s .